

**Deanship of Graduate Studies
Al-Quds University**

**Atomic Force Microscopy Study of the Electrical
Properties of Protein-Gold Nanoparticle Hybrids**

Mai Ibrahim Khalil Al-Maghalseh

M.Sc. Thesis

Jerusalem - Palestine

2009

Atomic Force Microscopy Study of the Electrical Properties of Protein-Gold Nanoparticle Hybrids

Prepared by:
Mai Ibrahim Khalil Al-Maghalseh

B.Sc. Physics. Al-Quds University-Palestine

Supervisor: Dr. Mukhles Sowwan

A thesis Submitted in Partial fulfillment of requirements for the degree of Master of Physics Program at Faculty of Physics, Al- Quds University.

2009



Thesis Approval

**Atomic Force Microscopy Study of the Electrical Properties of
Protein-Gold Nanoparticle Hybrids**

Prepared by: Mai Ibrahim Khalil Al-Maghalseh
Registration No.: 20714134

Supervisor: Dr. Mukhles Sowwan

Master thesis submitted and accepted, Date: **6/9/2009**

The names and signatures of the examining committee members are as follows:

1-Head of Committee:	Dr. Mukhles Sowwan	Signature	
2-Internal Examiner:	Dr. Jamal Ghaboun	Signature	
3-External Examiner:	Dr. Edward Sader	Signature	

Jerusalem – Palestine

2009

Dedication

This thesis is dedicated to my wonderful parents, Ibrahim and Maryam, who have raised me to be the person I am today. They have been with me every step of the way, through good times and bad. Thank you for all the unconditional love, guidance, and support that you have always given me, helping me to succeed and instilling in me the confidence that I am capable of doing anything I put my mind to. Thank you for everything. I love you!

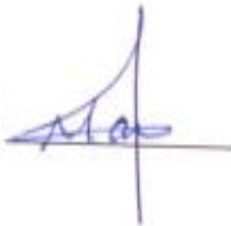
Also I want to dedicate this thesis to my fiancé Anas for his love, patience, and his unending support along the way.

Mai Ibrahim Khalil Al-Maghalseh

Declaration:

I certify that this thesis submitted for the degree of Master is the result of my own research, except where otherwise acknowledged, and that this thesis (or any part of the same) has not been submitted for a higher degree to any other university or institution.

Signed:

A handwritten signature in blue ink, appearing to be 'M. Al-Maghalseh', written over a horizontal line. A vertical line extends downwards from the end of the signature.

Mai Ibrahim Khalil Al-Maghalseh

Date: 6/9/2009

Acknowledgements

I would like to formally thank:

Dr. Mukhles Sowwan, my advisor, for his work and guidance throughout this entire research process. I have learned so much. Thank you so much for a great experience.

Dr. Jamal Ghabboun, for his great hard work and support and for believing in my abilities. Thank you so much for your insight and guidance throughout the past year.

Izhar Medalsy, for his support and help through analyzing the results. Thank you so much for the great help.

My best friend Maryam Faroun, for her friendship and support. The last two years have been quite an experience and you have made it a memorable time of my life. I will miss you. Good luck to you in your future endeavors.

My parents, for their never-ending love and support in all my efforts, and for giving me the foundation to be who I am. Thank you.

My sisters and brothers, Ghadeer, Husam, Haneen, Khalil, Hadeel, Salsabeel, and Ansam, for their love and support throughout the years. Thank you for the laughing and the fighting, and everything in between.

Anas, my soul mate and confidant, for always being there for me. Thank you for your continual love, support, and patience as I went through this journey. I could not have made it through without you by my side.

Abstract

In the last decade, molecular nanoelectronics gained a growing attention in the field of electronic devices because of the need to have new devices with characteristics that overlap the limitations and disadvantages of the existed devices fabricated with common methods. In order to achieve building electronic devices using biological molecules it will be necessary to measure, control and understand the electron transport through these molecules. The purpose of this research was to study the morphological characteristics of a ring shaped like protein named stable protein 1 (SP1), and a building block that consists of gold nanoparticles (GNP) embedded in the central cavity of the SP1 protein. The morphological characteristics was studied on different four substrates which are mica, silicon, gold, and HOPG using Atomic Force Microscopy with its two modes; tapping and contact. Another aim of this research was to study the electrical characteristics of the SP1 and the building block (SP1-GNP) by performing direct electrical measurements for these molecules on HOPG substrate using conductive Atomic Force Microscopy measurement technique.

AFM results revealed that the average heights of SP1 molecules on mica and silicon were 2.4 ± 0.3 and 2.2 ± 0.2 nm respectively, while on gold and silicon SP1 monolayer was formed with average height equal to 2 ± 0.1 nm. For SP1-GNP molecules their average heights were found to be 3.7 ± 0.4 nm and 3.3 ± 0.1 nm on mica and silicon respectively, but on gold and HOPG substrates a monolayer of SP1-GNP molecules was formed with average height of 4 ± 0.2 nm above both substrates. The results of the direct electrical measurements showed an insulating current-voltage curves with different voltage ranges for both SP1 and SP1-GNP molecules when force-distance mode was performed with small load (Normal Force). The current-voltage curves performed with high load (N.F) showed a semiconductor behavior for SP1 molecules and an ohmic behavior for SP1-GNP molecules.

Table of Contents

1. Introduction and Motivation	1
2. Methods and Materials	7
2.1 Atomic Force Microscopy.....	8
2.1.1 The Operation Principle of AFM.....	9
2.1.2 AFM Tips.....	10
2.1.3 Imaging Modes.....	11
2.2 Electrostatic Force Microscopy.....	13
2.3 Force vs Distance.....	14
2.4 Experimental Setup.....	15
2.5 Materials.....	16
2.5.1 SP1 Protein and SP1-GNP Complex.....	16
2.5.2 Substrates.....	19
2.6 Samples Preparation.....	20
2.6.1 SP1 Samples Preparation.....	20
2.6.2 SP1-GNP's Samples Preparation.....	20
3. Results and Discussion.....	21
3.1 Annealing of gold substrate.....	22
3.2 Morphological characterization of 73Cys-SP1 and 6His-SP1- GNP molecules.....	23
3.2.1 Morphological characterization of 73Cys-SP1 molecules on mica substrate.....	23
3.2.2 Morphological characterization of 73Cys-SP1 molecules on silicon substrate.....	26
3.2.3 Morphological characterization of 73Cys-SP1 molecules on gold substrate.....	28
3.2.4 Morphological characterization of 73Cys-SP1	

	molecules on HOPG substrate.....	29
3.2.5	Morphological characterization of 6His-SP1-GNP molecules on mica substrate.....	30
3.2.6	Morphological characterization of 6His-SP1-GNP molecules on silicon substrate.....	32
3.2.7	Morphological characterization of 6His-SP1-GNP molecules on gold substrate.....	34
3.2.8	Morphological characterization of 6His-SP1-GNP molecules on HOPG substrate.....	35
3.3	Electrical characterization of 73Cys-SP1 and 6His-SP1-GNP molecules.....	39
4.	Conclusion and Future Work.....	48
4.1	Conclusion.....	49
4.2	Future Work.....	49
	References.....	50

List of Figures

Figure Number	Figure Name	Page
Figure 1.1	<i>Plot of CPU transistor counts against dates of introduction.</i>	3
Figure 2.1	<i>Forces between the AFM tip and the sample as a function of the tip-sample distance.</i>	8
Figure 2.2	<i>A schematic representation of AFM main components of the system.</i>	9
Figure 2.3	<i>SEM images of AFM tips.</i>	10
Figure 2.4	<i>A schematic of Electrostatic Force Microscopy operation.</i>	13
Figure 2.5	<i>A force distance plot showing tips deflection in each point above the sample, a snap-in and a pull-off point are not in the same distance due to capillary forces acting on the tip forcing to apply bigger load to disconnect the tip from the surface.</i>	14
Figure 2.6	<i>A schematics of the experiment setup.</i>	15
Figure 2.7	<i>(a) SPI monomer with N-termini, (b) SPI dimer composed of two SPI monomers, (c) Crystal structure of SPI molecule with 12 N-termini, (d) Electron microscopy of SPI molecule.</i>	17
Figure 2.8	<i>(a) SPI monomer with Cys group, (b) Cys groups on SPI dodecamer, (c) SPI monomer with His group on N-termini, (d) His groups on 6 N-termini of SPI dodecamer, (e) GNP bind to the center of SPI molecule, (f) 3D image of SPI-GNP complex.</i>	18
Figure 3.1	<i>AFM topography images of (a) gold before annealing process; scanning size $1 \times 1 \mu\text{m}^2$, (b) and (c) after annealing; scanning size $4 \times 4 \mu\text{m}^2$, (d) Au (111) terraces after annealing.</i>	22

Figure 3.2	<i>AFM topography images of 73Cys-SPI molecules on mica substrate on different areas, acquired in tapping mode: (a) $2 \times 2 \mu\text{m}^2$, (b) $1 \times 1 \mu\text{m}^2$, (c) $1 \times 1 \mu\text{m}^2$, and (d) height profiles of SPI molecules.</i>	24
Figure 3.3	<i>(a) AFM topography image of 73Cys-SPI molecules on mica substrate, (b) flooding image of the topography (a) shows the SPI molecules with heights range from 2 nm to 3.3 nm, (c) height distribution for the SPI molecules in image (a), and (d) histogram shows height distribution of SPI molecules in the flooding image (b).</i>	25
Figure 3.4	<i>AFM topography images of 73Cys-SPI molecules on silicon substrate on different areas, acquired in tapping mode: (a) $2 \times 2 \mu\text{m}^2$, (b) $1.2 \times 1.2 \mu\text{m}^2$, (c) $700 \times 700 \text{ nm}^2$, and (d) height profiles of SPI molecules.</i>	26
Figure 3.5	<i>(a) AFM topography image of 73Cys-SPI molecules on silicon substrate, (b) flooding image of the topography (a) shows the SPI molecules with heights range from 2 nm to 2.6 nm, (c) height distribution for the SPI molecules in image (a), and (d) histogram shows height distribution of SPI molecules in the flooding image (b).</i>	27
Figure 3.6	<i>AFM topography images of 73Cys-SPI molecules on annealed gold substrate, on different areas, acquired in tapping and contact modes, the scratched regions were done using Si OMLC-AC tip, and the cross-section height profiles of the scratched areas: (a) $2 \times 2 \mu\text{m}^2$, (b) $3.2 \times 3.25 \mu\text{m}^2$, (d) and (e) $1.5 \times 1.5 \mu\text{m}^2$, (g) and (h) $1.2 \times 1.2 \mu\text{m}^2$.</i>	28
Figure 3.7	<i>AFM topography images of 73Cys-SPI molecules on HOPG substrate on different areas, acquired in tapping mode: (a) $2 \times 2 \mu\text{m}^2$, (b) height profile, (c) $1.1 \mu\text{m}^2$, and (d) $600 \times 600 \text{ nm}$.</i>	29
Figure 3.8	<i>AFM topography images of 6His-SPI-GNP molecules on mica substrate on different areas, acquired in tapping mode: (a) and (b) $1.4 \times 1.4 \mu\text{m}^2$, (c) $600 \times 600 \text{ nm}^2$, and (d) height profiles of 6His-SPI-GNP molecules.</i>	30
Figure 3.9	<i>(a) AFM topography image of 6His-SPI-GNP molecules on mica substrate, (b) flooding image of the topography (a) shows the SPI-GNP molecules with heights range from 2.5 nm to 10.7 nm, (c) height distribution for the SPI-GNP molecules in image (a), and (d) histogram</i>	31

- shows height distribution of the SPI-GNP molecules in the flooding image (b).*
- Figure 3.10 *AFM topography images of 6His-SPI-GNP molecules on silicon substrate on different areas, acquired in tapping mode: (a) 2x2 μm^2 , (b) 1.4x1.4 μm^2 , (c) 700x700 nm^2 , and (d) height profiles of 6His-SPI-GNP molecules.* 32
- Figure 3.11 *(a) AFM topography image of 6His-SPI-GNP molecules on silicon substrate, (b) flooding image of the topography (a) shows the SPI molecules with heights range from 2.5 nm to 6.3 nm, (c) height distribution for the SPI-GNP molecules in image (a), and (d) histogram shows height distribution of SPI-GNP molecules in the flooding image (b).* 33
- Figure 3.12 *AFM topography images of 6His-SPI-GNP molecules on annealed gold substrate, on different areas, acquired in tapping and contact modes, the scratched region was done using Si ElectriMulti75-G tip, and the cross-section height profile of the scratched area: (a) 4x4 μm^2 , (b) 3x3 μm^2 , (d) and (e) 1.5x1.5 μm^2 .* 34
- Figure 3.13 *AFM topography images of 6His-SPI-GNP molecules on HOPG substrate, on different areas, acquired in tapping and contact modes, the scratched region was done using Si ElectriMulti75-G tip, and the cross-section height profile of the scratched area: (a) 800x800 nm^2 , (b) 500x500 nm^2 , and (c) 1.5x1.5 μm^2 .* 35
- Figure 3.14 *A schematic of SPI and SPI-GNP standing tubes.* 38
- Figure 3.15 *F-d curves (a) with high normal force, (b) with small normal force on bare gold; the green and red lines represent approach and withdrawal deflection of the oscillated tip respectively; in the last point of the approach, the I-V measurements can be performed; the slope of the red line in (b) shows the presence of adhesion and capillary forces between the tip and the gold.* 40
- Figure 3.16 *Results of the combined F-d/ I-V mode on bare gold, (a) F-d curve on gold with small normal force of the tip on the sample, and (b) I-V curve for gold with voltage sweep from -1.5v to 1.5v.* 40

Figure 3.17	<i>Result of the combined F-d/ I-V mode on SPI molecules, (a) SPI molecules that the measurements have been done on, (b) no pressing in F-d curve (green line), and (c) 10 I-V curves with zero current and voltage sweep from -1.5v to 1.5v.</i>	41
Figure 3.18	<i>Result of the combined F-d/I-V mode on SPI-GNP molecules showed, (a) SPI-GNP molecules that the measurements have been done on, (b) no pressing in F-d curve (green line), and (c) 10 I-V curves with zero current and voltage sweep from -2v to 2v.</i>	42
Figure 3.19	<i>Result of the combined F-d/I-V mode on SPI molecules, (a) SPI molecules that the measurements have been done on, (b) pressing in F-d curve, the SPI molecule is pushed to direct contact with the HOPG substrate, and (c)-(f) the I-V curves with sweep voltage from -1.5v to 1.5v and -2v to 2v.</i>	43
Figure 3.20	<i>Result of the combined F-d/I-V mode on SPI-GNP molecules, (a) SPI-GNP molecules that the measurements have been done on, (b) pressing in F-d curve, the GNP is pushed to direct contact with the HOPG substrate, and (c)-(f) the I-V curves with sweep voltage from -2v to 2v.</i>	44
Figure 3.21	<i>A comparison between two I-V curves, (a) for SPI molecule showing sigmoidal shape, (b) for SPI-GNP molecule showing an ohmic signal.</i>	45
Figure 3.22	<i>A schematic of metal-protein-metal junction.</i>	46
Figure 3.23	<i>A schematic of a nanowire from SPI-GNP molecules.</i>	47

List of Tables

Table Number	Table Name	Page
Table 3.1	The dimensions of SP1 and SP1-GNP molecules obtained by different methods.	36
Table 3.2	The dimensions of SP1 and SP1-GNP molecules obtained by AFM tapping mode on different four substrates.	37
Table 3.3	Electrical prosperities of SP1 and SP1-GNP molecules obtained by EFM and I-V.	45

Abbreviations

STM	Scanning Tunneling Microscopy
SPM	Scanning Probe Microscopes
AFM	Atomic Force Microscopy
DNA	Deoxyribonucleic Acid
NP	Nanoparticle
GNP	Gold Nanoparticle
SP1	Stable Protein One
EFM	Electrostatic Force Microscopy
His	Histidine
Cys	Cystein
HOPG	Hydrophobic Highly Oriented Pyrolytic Graphite
PSD	Position Sensitive Detector
DSP	Digital Signal Processing
VDW	Van der Waals
F-d	Force versus Distance
JIC	Jump In (To) Contact or “Snap-In” Point
C-AFM	Conductive AFM
I-V	Current- Voltage
KDa	Kilodalton
N.F	Normal Force
T.D.W	Triple Distilled Water

Chapter ONE

Introduction and Motivation

Chapter ONE

Introduction and Motivation

The technological development came as a result of human efforts and his way of thinking in using information, skills, experiences, and elements in any area to discover and develop heuristics that can solve his problems, satisfy his needs, and increase his abilities.

One of the most important fields which has witnessed the technological evolution is the field of electronic devices. The history of electronics began when the vacuum tube was invented by Dr Lee Deforest in 1907 (McChesney 1994), which was developed to a device that can amplify electrical signals. In 1947 Bell laboratory researchers invented the first solid state device which is the transistor. The idea of the transistor based on controlling the flow of the electrons through a material like silicon by designing some areas as conductors and others as insulators (Rosenbloom and Spencer 1996). After eleven years Jack Kilby invented the integrated circuit which composed of a number of transistors integrated in the body of the semiconductor material (Dummer 1997).

Through years of hard work and effort to develop new methods to fabricate electronic devices, planar process was innovated and the history of the exponential growth in the field of electronics began. In 1959 this process enabled Fairchild physicist Jean Hoerni to produce the first planar transistor and to make the electrical connections by depositing and evaporating metal film on preferable parts of the semiconductor wafer instead of using hands (Hoerni 1961). By the year 1961 the first planar integrated circuit was produced by Fairchild. Then the number of transistors in the integrated circuits began to increase each year. In 1965 the co-founder Intel Corporation Gordon E. Moore noticed that the number of transistors which can be placed in an integrated circuit has increased exponentially, doubling approximately every two years according to the relation:

$$\text{(Circuit per chip)} = 2^{(\text{year} - 1975) / 1.5}$$

scientists did not stop at this limit. They went farther and started thinking how to improve the quality of these electronic devices like increasing the speed of computer calculations. The answer was reducing the electron flight time through the chip by reducing the chip size, which was the reason in the birth of lithographic technologies that lead to downsized the electronic devices from 2 μm to 0.18 μm (Geppert 1999). Through this revolution in the world of electronic devices, some scientists were busy in studying the physical prosperities of systems. They noticed the change in some physical properties of materials and systems when going to a new scale called nano.

In 1959 the first concepts of nano was presented by Richard Feynman in his lecture “There’s Plenty of Rooms at the Bottom” at the annual meeting of the American Physical Society at the California Institute of Technology (Feynman 1960). Thus a new era of technology appeared, the era of nanotechnology, which was defined by Tokyo Science University Professor Norio Taniguchi in 1974 as: ” Nano-technology mainly consists of the processing of separation, consolidation, and deformation of materials by one atom or by one molecule” (Taniguchi 1974). According to NASA Ames Research Center, nanotechnology is defined as the creation of functional materials, devices and systems through control of matter in the range of one-tenth to one-hundred nanometer (0.1-100 nm) and the exploitation of novel phenomena and properties in this scale, while the prefix nano represents 10^{-9} , i.e., one billionth of a unit (NOVA Workforce Board 2003).

The start of the nanotechnology and nanoscience began with the invention of Scanning Tunneling Microscopy (STM) by Gerd Binnig and Heinrich Rohrer, and the invention of Atomic Force Microscopy (AFM) after six years (Binnig 1986). In the 1980s the dream of molecular technology was introduced by Dr. K. Eric Drexler in his book “Engines of Creation”. The dream was about the ability to achieve the control in operation, perfection in construction, and variety in design, by assembling biological systems and devices at the molecular levels (Drexler 1986). Thus molecular electronics came with its three features; recognition, structuring, and electrical functionality (Fabio 2004); that is biology molecules recognize each other, have the ability to bind to one another, assemble into larger structures and transport efficiency carriers from one point to another. These three features allow the

molecular electronics to overlap the limitations of e-beam lithography in fabricating electronic devices which are the huge cost of starting up such technique, the physical limitations of the raw materials which is silicon, and the diffraction limitation (Iwai and Ohmi 2002).

Following the invention of Scanning Probe Microscopes (SPM), there were many published works about the deoxyribonucleic acid (DNA) and proteins assembly of nanometer and micrometer scale structures that can have a profound impact in the fields of nanoelectronics and nanotechnology and the potential to continue the scaling of Moore's law beyond the 50 nm node (Bashir 2001). In the year 1999 the controlled conjugation of Au nanoparticles single-stranded DNA was achieved by Maeda et al. The AFM was used to confirm the one-to-one binding of Au nanoparticles to plasmid DNA (Maeda 1999). The measurements of the electrical conductivity of metallic nanowires fabricated by chemical deposition of a thin continuous palladium film onto single DNA molecules confirmed that DNA is an ideal template for the production of electric wires, which can be utilized for the bottom-up construction of miniaturized electrical circuits (Richter 2001). In 2002, McMillan et al presented the fabrication of nanoscale ordered arrays of metal and semiconductor quantum dots, by binding preformed nanoparticles onto crystalline protein templates made from genetically engineered hollow double-ring structures called chaperonins, which demonstrated that quantum dots can be manipulated using modified chaperonins and organized into arrays for use in next-generation electronic and photonic devices (McMillan 2002). Macrocycles, DNA quadrilateral, DNA knots, Holliday junctions, and other structures were designed by Seeman using branched DNA and choosing the sequence of the complementary strands (Seeman 2003).

The construction of two-dimensional and periodical gold nanoparticle arrays using a new DNA-NP conjugate system that allows Au NPs to be readily assembled onto a DNA tiling system was developed by Sharma et al, the thing that paved the way for the assembly of more complex nanoparticle arrays on DNA nanoscaffolds for future device applications (Sharma 2006). Nanoelectronic concept based on protein-nanoparticle hybrids was implemented by Medalsy et al (Medalsy 2008). He was able to develop a building block for

Lego like fabrication of nanoelectronic devices, in which gold Nanoparticles (GNP) are embedded in the central cavity of a ring shaped like protein that is named stable protein 1 (SP1). The Electrostatic Force Microscopy (EFM) studies showed that the bare SP1 is electrically silent while the SP1 gold hybrid is polarized. Tapping mode AFM topographic characterization was also performed by Medalsy et al on 6His-SP1 and on GNP-bound 6His-SP1 deposited on freshly cleaved mica surfaces. The results showed an average heights of 2.3 ± 0.2 nm and 3.3 ± 0.2 nm for the 6His-SP1 and for the GNP-bound 6His-SP1, respectively. Moreover he used 6HisSP1 GNP hybrids to form protein-GNP chains with different GNP separations. Also a highly ordered and continuous array of Wild type SP1 (W.T. SP1) was formed too (Medalsy 2008).

In order to achieve building an electronic device using individual molecules such as SP1 and SP1-GNP hybrid it will be necessary to measure, control and understand the electron transport through these molecules. My work in this research includes two parts. The first part is studying the morphological characteristics of 73Cys-SP1 and 6His-SP1-GNP hybrids on mica, silicon, HOPG, and gold substrates, where Cys and His are mutants added to the SP1 molecule by genetic engineering. The second part is studying the electrical properties of both 73Cys-SP1 and 6His-SP1-GNP on HOPG substrate by direct electrical measurements. The main tool that I have used through my research is the AFM instrument, with two kinds of AFM conductive tips. Tapping and Contact are the main AFM modes which were used for morphological characterization of SP1 and SP1-GNP molecules, while the direct electrical measurements were performed using the combined force-distance/ current- voltage mode..

This thesis includes four chapters; Chapter one is a general introduction and Motivation. Chapter two includes methods and materials used throughout this work. An introduction to the atomic force microscopy; the main instrument and technique used in this study available in our laboratory, and its different modes of operation are outlined as well as in chapter two. Measurements collected throughout the research phases are reported and discussed with details in chapter three. Finally, conclusion, suggested future work are registered in chapter four.

Chapter TWO

Methods and Materials

Chapter Two

Methods and Materials

2.1 Atomic force microscopy (AFM)

Microscopes have historically been tools of great importance in research. The Atomic Force Microscopy (AFM) is one of a family of Scanning Probe Microscopes (SPM) which has grown steadily since the invention of the Scanning Tunneling Microscope (STM) by Binnig and Rohrer in the early eighties for which they received the Nobel Prize in Physics in 1986 (Binnig 1986). Later it has become the most popular scanning probe technique since it enables us to have a look on surfaces on a molecular level in several modes. Moreover, it overcomes the limitation of STM in imaging thin samples on electrically conductive materials. In addition to the high resolution, AFM offers the possibility to map electronic, mechanical, and optical properties.

All the microscopes from the SPM family, including AFM, work on the same principle; a probe is scanned above the surface at a distance where a specific interaction is present between them and monitored by a feedback loop. The interactions in AFM are usually based on the forces acting between a probe and a sample, Fig. 2.1.

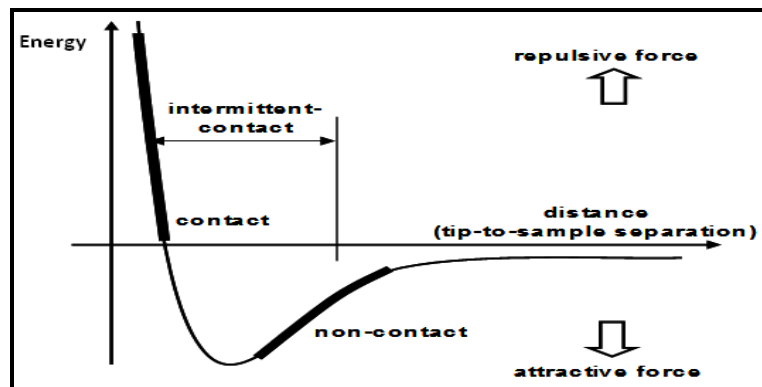


Fig. 2.1: Forces between the AFM tip and the sample as a function of the tip-sample distance, adapted from <http://www.e13.physik.tu-muenchen.de>.

2.1.1 The operation principle of AFM

The tip/probe placed on a cantilever. The laser and the position sensitive detector (PSD) which follows the deflection of the cantilever, a piezoelectric scanner which holds the sample and AFM electronics for operating all components together are the main components of the AFM, Fig. 2.2.

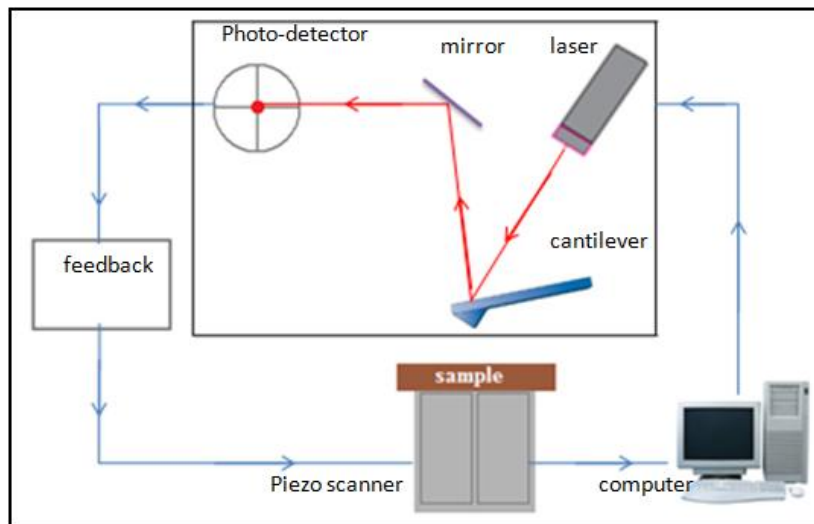


Fig. 2.2: A schematic representation of AFM main components of the system.

The tip is placed at a working distance above the surface and an image is acquired by moving the sample relative to the tip by means of piezo tube which changes its length (distortion in XY or Z axis with sub Angstrom resolution) upon voltage application. The forces acting between the tip and the sample lead to a cantilever deflection, depending on the tip-sample attractive or repulsive interactions that includes changes in the working distance. To keep the working distance constant, the relative tip-sample position is adjusted by the feedback loop. The topography of the scanned surface is reconstructed, e.g., by analyzing the deflection of the cantilever through measuring the position of the reflected laser beam on the PSD.

AFM electronics– a control workstation- have the digital signal processing (DSP) card which holds the information for the X-Y-Z scan, and bias voltage between tip and sample.

These signals are low-voltage signals and are converted to high-voltage (HV) signals in the HV box. DSP also receives the signals of the normal, lateral forces and the sum of the photodiode intensities coming from the head and through the HV box.

2.1.2 AFM tips

The tips used in this research are of two categories; (OMLC-ACTM, Olympus) and (ElectriMulti75-GTM, Budget-Sensor). The first one is a rectangular Si cantilever (30 x 240 μm), coated with Pt conductive layer, with spring constant of 2 N/m. The tip has a sharpened tetrahedral shape with apex of 15 nm. The other one is a rectangular Si cantilever (28 x 225 μm), coated with Cr-Pt conductive layer, with spring constant of 1.9 N/m. The tip has a three-pyramidal shape with apex of 15 nm. Both tips were used for morphological characterization, while the direct electrical measurements (I-V) were performed using ElectriMulti75-G, Fig. 2.3 shows SEM images of the different tips that were used.

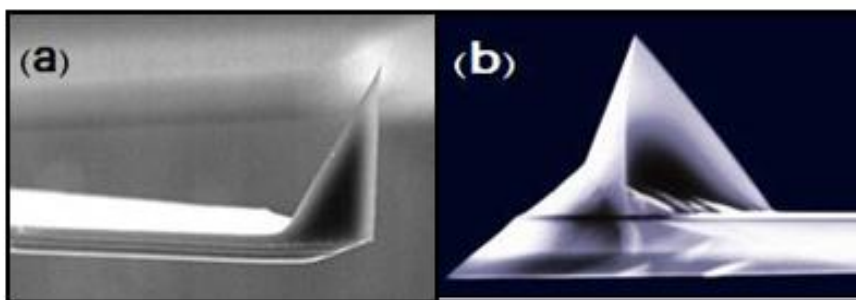


Fig. 2.3: SEM images of AFM tips; (a) Side view SEM image of OMLC-AC Si tip, adapted from *probe.olympus-global.com*. (b) SEM image of ElectriMulti75-G tip, adapted from *sigmaaldrich.com*.

2.1.3 Imaging modes

The purpose of this subsection is to describe the operation principles of the main modes of the AFM, as shown in Fig. 2.1. The main ranges of operation in AFM are determined according to the distance between the tip and the sample: contact, non-contact, and tapping modes.

a- Contact and non- contact modes

In contact mode, physical contact between the tip and the sample is established. The working point of the scanning is the point of constant tip deflection, meaning constant force applied between the tip and the sample. The changes in topography during the scanning, cause bending of the cantilever which is recorded by PSD and corrected by the feedback to keep a constant deflection. At the same time, the deviations in the cantilever deflection are analyzed to produce an image of the topography of the surface. Contact mode has the disadvantage of damaging soft samples, the so called "disadvantage" of the contact mode was used for estimating the height of samples layers created above the modified surfaces.

In non-contact mode, the distance between the tip and the sample is one to several tens of nanometers in the van der Waals force range. At relatively large tip-surface separation, the detection method is more sensitive to force gradient than to the interaction forces. The force applied by the tip on a sample is in the order of pico Newton (10^{-9} N) which enables imaging of soft biological samples, but cause small to no changes in the tip deflection.

In non-contact AFM mode, the tip-sample interactions are measured using a vibrating tip. If the tip vibrates at a distance outside the van der Waals interactions, then it has free resonance vibration frequency, determined by its force constant (k). When the tip comes into interaction with the surface, the attractive interactions lead to changes of the force constant, depending on the tip-sample separation, to a shift in the resonance frequency and as a consequence to attenuation of the vibration amplitude. Thus, the vibration amplitude is a measure of the distance of the tip from the sample surface. The working point of non-contact mode is the constant amplitude of the tip in a relatively close distance from the sample where tip-sample interactions are traceable.

b- Tapping mode

Tapping mode is another mode of operation for AFM, which is a patented technique that maps topography by lightly tapping the surface with an oscillating probe tip. In tapping mode the cantilever assembly at or near the cantilever's resonant frequency using a piezoelectric scanner. The piezo motion causes the cantilever to oscillate with a high amplitude when the tip is not in contact with the surface. The oscillating tip is then moved toward the surface until it begins to lightly touch, or tap the surface. As the tip is scanned over the surface, the cantilever is driven at its resonant frequency (hundreds of kHz). Because the contact time is a small fraction of its oscillation period, the lateral forces are reduced dramatically.

Tapping Mode has become an important AFM technique, as it overcomes some of the limitations of both contact and non-contact AFM modes. By eliminating lateral forces that can damage soft samples and reduce image resolution, tapping mode allows routine imaging of samples once considered impossible to image with AFM, especially in contact mode. Moreover tapping mode is related to limitations that can arise due to the thin layer of liquid that forms on most sample surfaces in an ambient imaging environment, i.e., in air or some other gas. The amplitude of the cantilever oscillation in tapping mode is typically on the order of a few 10's of nanometers, which ensures that the tip does not get stuck in this liquid layer, while the amplitude used in non-contact AFM is much smaller. Thus as a result, the non-contact tip often gets stuck in the liquid layer unless the scan is performed at a very slow speed.

In general, tapping Mode is much more effective than contact and non-contact modes for imaging larger scan sizes that may include large variations in sample topography. All of these advantages of tapping mode made it a suitable for morphological characterization of my samples through the research.

2.2 Electrostatic Force Microscopy (EFM)

Electrostatic Force Microscopy (EFM) is one of the AFM modes which maps electric properties on a sample surface by measuring the electrostatic force between the surface and a biased AFM cantilever. EFM applies a voltage between the tip and the sample while the cantilever hovers above the surface, not touching it. The cantilever deflects when it scans over static charges, as depicted in Fig. 2.4.

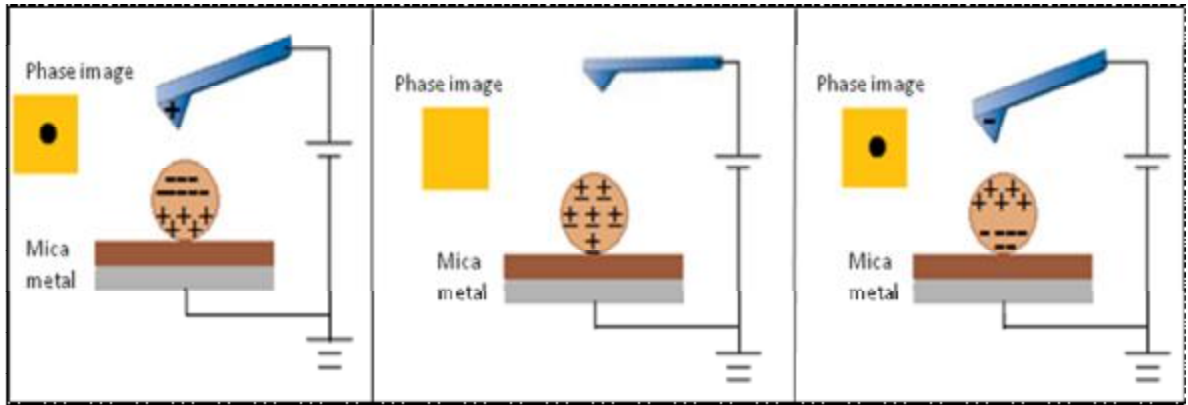


Fig. 2.4: A schematic of Electrostatic Force Microscopy operation.

For EFM, the sample surface properties would be electrical properties and the interaction force will be the electrostatic force between the biased tip and the sample. However, in addition to the electrostatic force, the van der Waals (vdw) forces between the tip and the sample surface are present. The magnitude of these vdw forces change according to the tip-sample distance, because of that when making topographic image for the surface the only force existed is the vdw forces and the obtained signal called (Topo signal). While the obtained signal to measure the surface electrical properties called (EFM signal) and generated by the electrostatic forces.

2.3 Force vs distance

Force versus distance (F-d), or force spectroscopy, in AFM allows investigating the forces acting between the tip and the surface. Additional valuable information can be provided from F-d plots, like the local mechanical properties of the surface or the hydrophobic/hydrophilic response of the material on the surface. The significance of the

force-distance mode in the present work is in controlling the applied force in each point above the sample. Applying large forces on a molecule can cause its distortion and, as a consequence, changes in the electrical properties of the molecule.

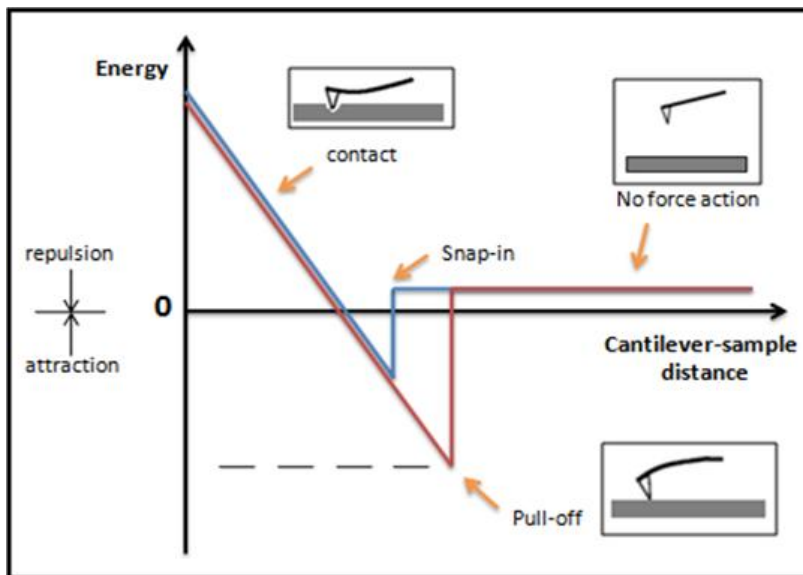


Fig. 2.5: A force distance plot showing tips deflection in each point above the sample, a snap-in and a pull-off point are not in the same distance due to capillary forces acting on the tip forcing to apply bigger load to disconnect the tip from the surface.

Fig. 2.5 shows a representative F-d plot measured during force spectroscopy when the tip-sample distance is reduced and the deflection of the tip is recorded in each point during the approach. During the initial approach of the sample to the tip (when the sample is placed on the piezoelectric unit), while the tip is in the region of no physical interaction with the surface, the tip deflection is constant. When the tip-sample distance is small enough, the tip jumps into contact with the surface as a result of the vdw forces acting on the tip (“snap-in” or “jump in (to) contact” Fig. 2.5). Further movement of the tip occurs in continuous contact with the sample. The value of the deflection in this part of the graph depends on the force constant k , of the cantilever. In the retracting curve, the piezoelectric unit withdraws the sample from the tip. The forces applied on the sample diminish till the “pull off” contact point. This point is different from the jump in contact (JIC) point because of the adhesive

and capillary forces acting on the tip in the atmosphere of relative humidity. In the “pull off” point the force applied by a piezo for retraction overcomes the capillary and adhesive forces of the sample and tip disconnects from the sample. Thus the cantilever returns to the initial position when small force (pN) is acting on the tip for topographic scanning.

2.4 Experimental setup

Samples includes 73Cys-SP1 and 6His-SP1-GNP's complex deposited on HOPG surface. Each SP1 molecule has 73 Cys, while in the complex of it with GNP's it has 6His, which enables both the SP1 molecules and their complex to be attached to different substrates like the HOPG surface, that is schematically presented in Fig. 2.6.

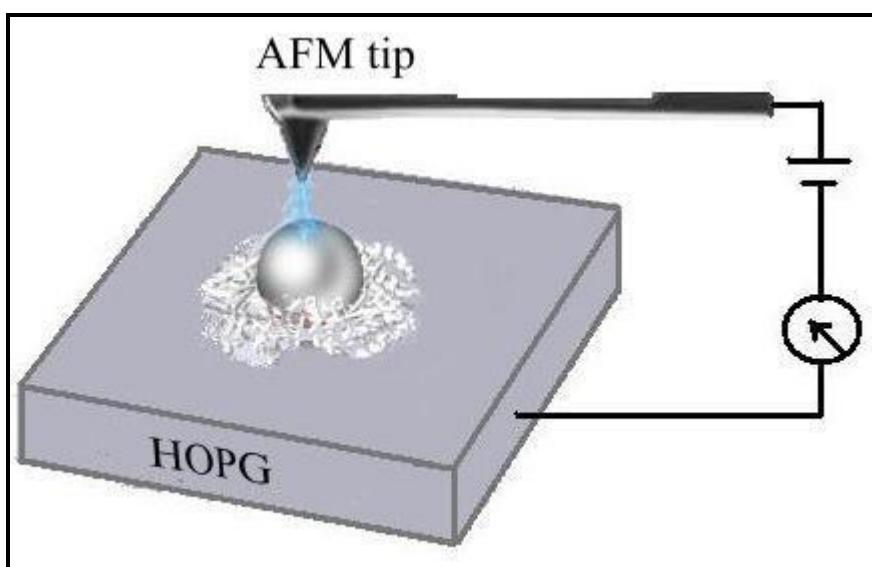


Fig. 2.6: A schematic of the experiment setup.

In the experimental configuration of this work, electrical contact to the SP1, 6His-SP1-GNP's was made with a C-AFM tip as one of the electrodes. Current-voltage characteristics of the sample were measured by applying voltage between the tip and the HOPG substrate which is the second electrode.

2.5 Materials

2.5.1 SP1 protein and SP1-GNP complex

Stable protein 1 (SP1) is a 108-amino-acid hydrophilic polypeptide with a molecular mass of 148.8 kDa (Wang 2002, 2003), isolated from aspen plants (*Populus tremula*) (Pelah 1995, 1997). It is boiling stable, stress-responsive protein with no significant sequence homology to other stress-related proteins (Dure 1993, Ingram 1996, Thomashow 1999), which suggest that SP1 represents a new class of stress-related proteins.

The SP1 molecule consist of 12 identical protein subunits, Fig. 2.7c, each subunit is called a monomer and of 12.4 KDa, Fig. 2.7a. The crystal structure of SP1 indicated strong hydrophobic interactions between two monomers that created a very stable dimer, Fig. 2.7b which spontaneously assemble into a uniform ring-like shape with diameter of 11 nm, inner pore of 2-3 nm and width of 4-5 nm, which is revealed by the X-ray crystallography studies (Dgany 2004).

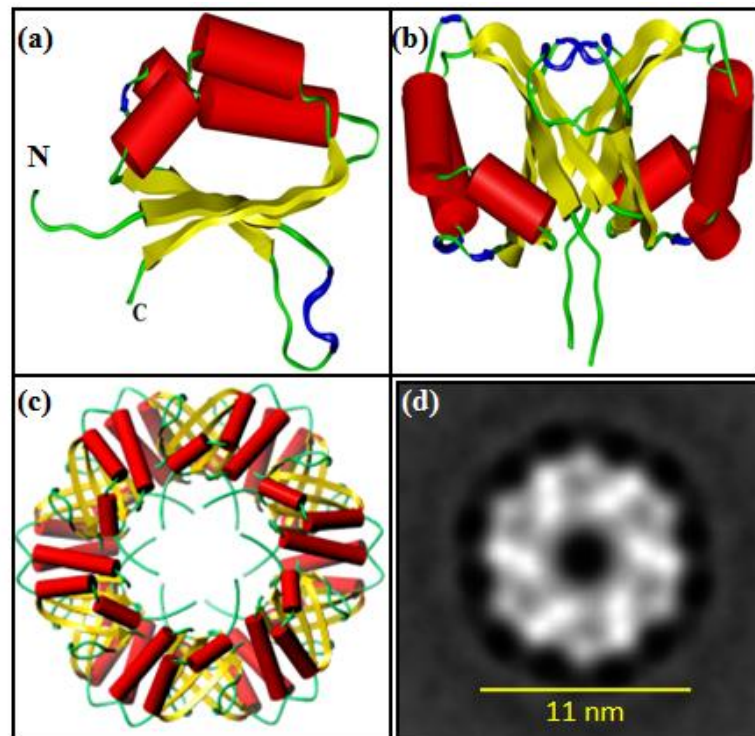


Fig. 2.7: (a) SP1 monomer with N-termini, (b) SP1 dimer composed of two SP1 monomers, (c) Crystal structure of SP1 molecule with 12 N-termini, (d) Electron microscopy of SP1 molecule.

The N-termini of the SP1 are pointing from the central cavity to the opposite planes of the ring in a way that 6 N-termini point to one side and the other 6 N-termini point to the opposite side as presented in Fig. 2.7, (a) and (c), (N-termini in green). Therefore, the SP1 protein can be modified by genetic engineering to enable it to bind in a flat orientation to the substrate underneath, and to the gold nanoparticle at the center on top of the SP1 ring. This can be done by adding mutants such as cysteine group (Cys) that can bind to the SP1 monomer and complex, and histidine group (His) that can bind to the 6 N-termini of the SP1 molecule which allowing the binding of GNP to it, Fig. 2.8.

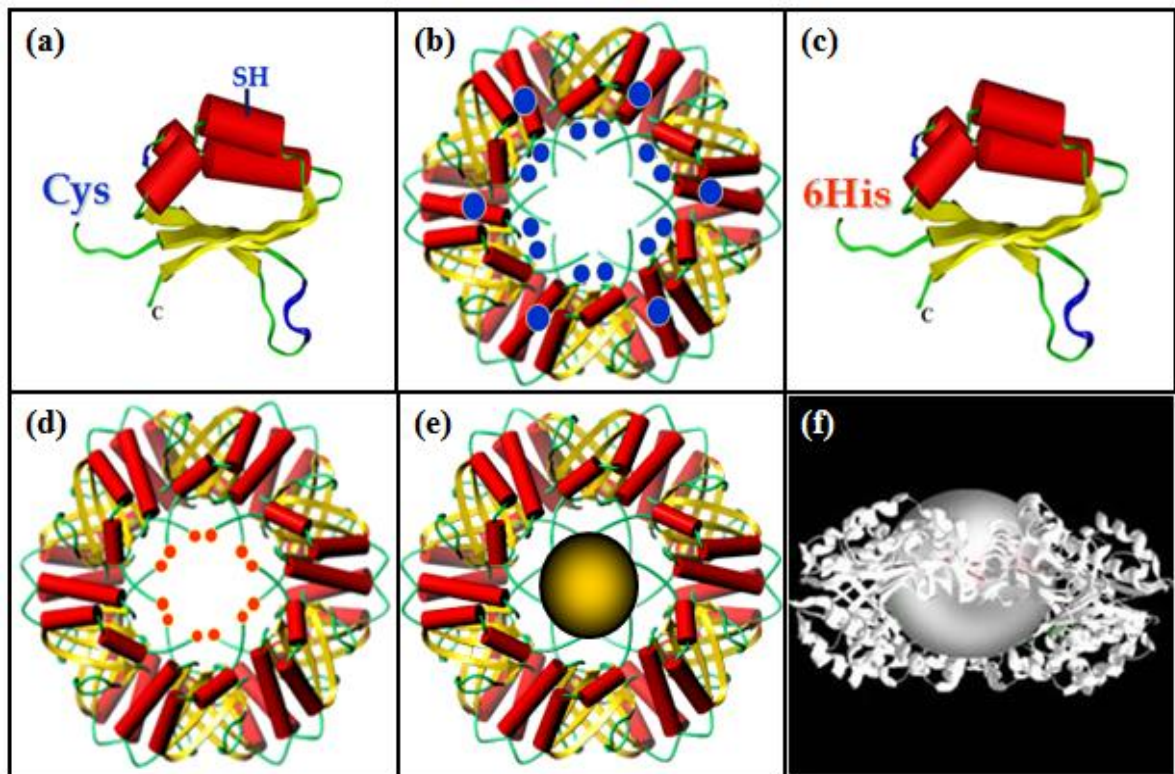


Fig. 2.8: (a) *SP1 monomer with Cys group*, (b) *Cys groups on SP1 dodecamer*, (c) *SP1 monomer with His group on N-termini*, (d) *His groups on 6 N-termini of SP1 dodecamer*, (e) *GNP bind to the center of SP1 molecule*, (f) *3D image of SP1-GNP complex*.

The SP1 protein has several properties that made from it a unique protein for many possible nanoelectronic devices such as molecular wires and ultra high density memory. These properties are the high stability, the resistant to high temperatures, high levels of ionic detergent, various proteases, and wide range of pH. Moreover the ring shape of SP1 with N-termini that can be modified by adding functional groups to allow it to bind to GNP and substrates (Medalsy 2008).

The SP1 protein solution, that is used in the experiment is prepared from original solution purchased from fulcrum SP1 Ltd, with concentration of 12.76×10^{-6} M. A new solution with concentration of 50 nM is prepared and used to prepare the samples. The 6His-SP1-GNP's solution that is used to prepare the samples has a concentration of 1.19 mg/ml and the GNP's used in this solution is of 1.8 nm in dimension. This solution was purchased from sigma-Aldrich Ltd.

2.5.2 Substrates

a- Mica

Mica is a hydrous silicates of aluminum and potassium, often containing magnesium, ferrous iron, ferric iron, sodium, and lithium and more rarely are containing barium, chromium, and fluorine. It is most commonly found in the form of sheets and can split into very thin elastic laminate. The entire mica surfaces can be easily updated by a simple cleaving, by first pressing some adhesive tape against the top mica surface, then peeling off the tape. In the experiment the thin mica sheets which were used purchased from SPI supplies, USA.

b- Gold

A commercial gold substrate (Gold Arrendee/ Au (111)), 200 nm thick, on borosilicate, with high rms roughness is annealed by a flame using highly refined butane gas. The substrate was cleaned first in acetone and then in ethanol in ultrasonic bath for 10 minutes. After drying the gold surface with Nitrogen gas, flame annealing was performed in a dark room for observation of the dark red glowing of the gold.

c- Silicon

A commercial Silicon wafer, silicon oxide one side coated and polished was purchased from Spi supplies. In order to remove the native oxide layer from the surface of silicon substrate, it was cleaned in ethanol in ultrasonic bath for 20 minutes.

d- HOPG

HOPG, is a Hydrophobic highly oriented pyrolytic graphite surface which is a new form of high purity carbon purchased from Spi supplies. In particular HOPG is described as consisting of a lamellar structure like mica so the entire surfaces can be easily updated by a simple cleaving using adhesive tape.

2.6 Samples preparation

The preparation of each sample includes two stages: the preparation of clean and flat substrate, and the deposition of the solution on the surface of the substrate.

2.6.1 SP1 samples preparation

All samples of the SP1 solution on the different four substrates were prepared with the same conditions. After preparing a clean and flat surface with the procedures mentioned above for

each substrate, 5 μ l of SP1 solution with concentration of 50 nM is deposited on the surface of the substrate, with incubation time of 15 minutes except for the HOPG surface, the incubation time was 5 minutes. After that, the sample washed with T.D.W and dried with Nitrogen gas. For the annealed gold substrate the SP1 solution is deposited right after the annealing and the sample was put in contact with a large metal block for cooling.

2.6.2 SP1-GNP's samples preparation

All the samples of the 6His-SP1-GNP's solution on the different four substrates were prepared with the same conditions. After the preparation of clean and flat surface, 5 μ l of 6His-SP1-GNP's solution with concentration of 1.19 mg/ml is deposited on the surface of the substrate, with incubation time of 5 minutes except for the HOPG surface, the incubation time was 1 minute. After that the sample was washed with T.D.W and dried with Nitrogen gas.

Chapter THREE

Results and Discussion

Chapter THREE

Results and Discussion

3.1 Annealing of gold substrate

Following the annealing procedure, mentioned in methods and materials in subsection 2.5.2, atomically smooth Au (111) terraces were obtained as shown in Fig. 3.1d. During the annealing, the microstructure of gold changed, and lead to the formation of large grains, 1 μm^2 to 4 μm^2 in size, Fig. 3.1.

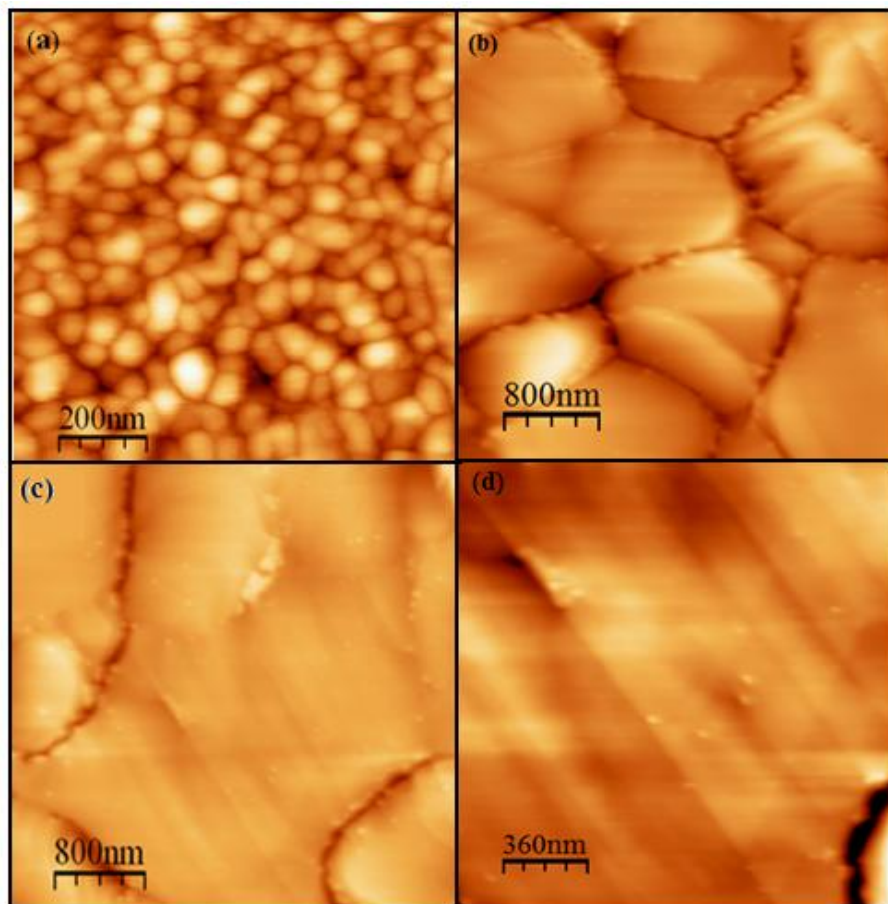


Fig. 3.1: AFM topography images of (a) gold before annealing process; scanning size $1 \times 1 \mu\text{m}^2$, (b) and (c) after annealing; scanning size $4 \times 4 \mu\text{m}^2$, (d) Au (111) terraces after annealing.

3.2 Morphological characterization of 73Cys-SP1 and 6His-SP1-GNP molecules

AFM tapping and contact modes were used to morphologically characterize the samples. All the images were obtained with a commercial AFM (Nanotec Electronica, Madrid) of ambient conditions. The OMLC-AC and ElectriMulti75-G tips were used for tapping and contact modes images. Scratching in contact mode was performed as one of the tests to verify the layers height above a flat gold and HOPG surfaces. In general, the AFM tip was put into contact with the surface of the substrate through the SP1 and SP1-GNP layers. During the scan, part of the layers was removed away. After the contact mode was completed, topography was done above the scratched area. Topography images show, in a profile, the

difference in height between the scratched and unscratched areas. The morphological and electrical results were collected in tables at the end of the morphological and electrical characterization sections.

3.2.1 Morphological characterization of 73Cys-SP1 molecules on mica substrate

The surface morphology on mica substrate was characterized using AFM tapping mode and OMLC-AC tip. Fig.3.2 shows different topography images of SP1 molecules on mica substrate with height profiles for some molecules.

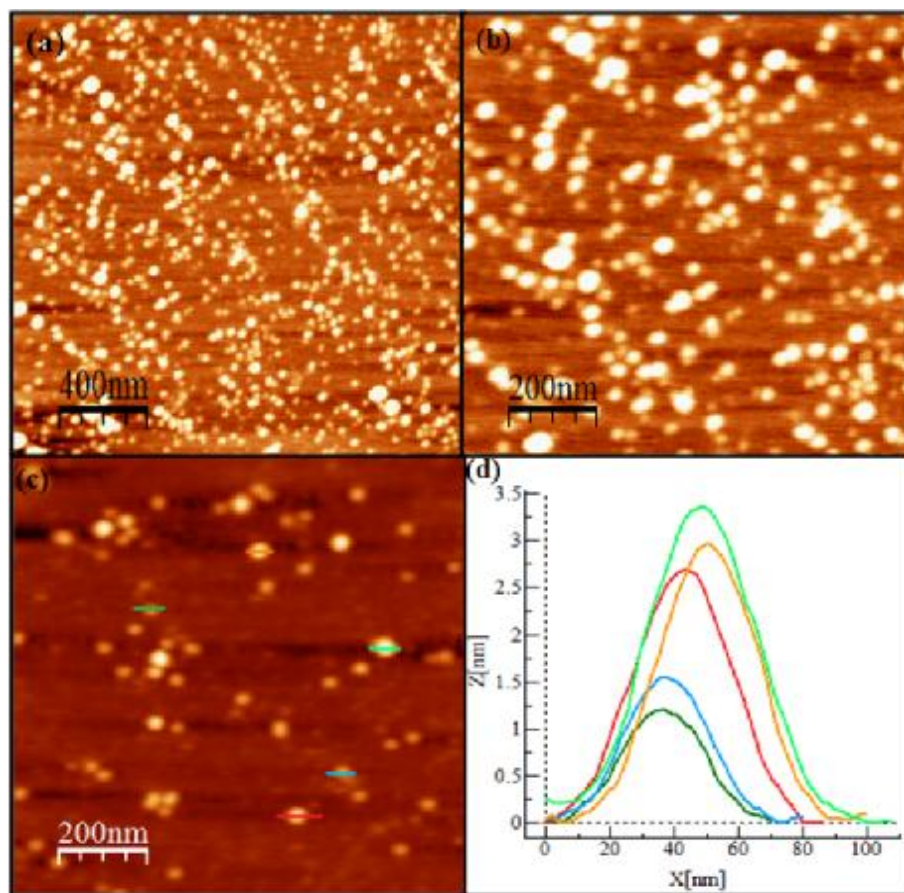


Fig. 3.2: AFM topography images of 73Cys-SP1 molecules on mica substrate on different areas, acquired in tapping mode: (a) $2 \times 2 \mu\text{m}^2$, (b) $1 \times 1 \mu\text{m}^2$, (c) $1 \times 1 \mu\text{m}^2$, and (d) height profiles of SP1 molecules.

From Fig. 3.2, the topographic images on different areas shows the SP1 molecules that bound to mica substrate. It is clear that SP1 molecules spread over the surface with different sizes and heights. The SP1 molecules on mica were found to have a diameter ranges from 30 nm to 40 nm, while the heights range from 1 nm to 3.3 nm.

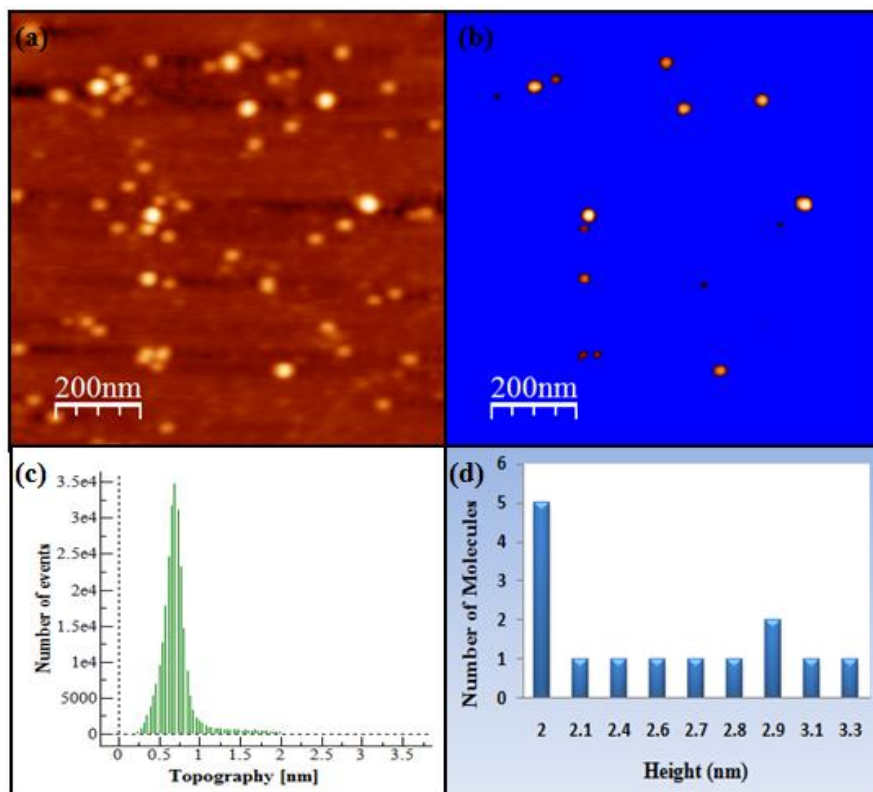


Fig. 3.3: (a) AFM topography image of 73Cys-SP1 molecules on mica substrate, (b) flooding image of the topography (a) shows the SP1 molecules with heights range from 2 nm to 3.3 nm, (c) height distribution for the SP1 molecules in image (a), and (d) histogram shows height distribution of SP1 molecules in the flooding image (b).

The topography image (a) in Fig. 3.3 shows all the SP1 molecules with different heights, while (b) is a flooding image* of the topography (a), which was performed to show only the SP1 molecules with minimum heights of 2 nm and more. The results obtained from the flooding image in Fig. 3.3b, and height distribution of the SP1 molecules in Fig. 3.3c, revealed that most of the SP1 molecules on mica surface are of heights less than 2 nm. These

* Flooding image: height filter image.

SP1 molecules with such heights have been neglected since they present SP1 fractions, i.e., SP1 molecules that lost some of their subunits. The histogram of heights which was performed on the molecules presented in the flooding image Fig. 3.3d, shows that most of SP1 molecules (5 molecules) are with height equal to 2 nm. It was found from the height profiles in Fig. 3.3d (performed on several dozens of SP1 molecules) that SP1 molecules on mica substrate are of average height 2.4 ± 0.3 nm.

3.2.2 Morphological characterization of 73Cys-SP1 molecules on silicon substrate

The surface morphology on silicon substrate was characterized using AFM tapping mode and OMLC-AC tip. With comparison between the topographic images obtained for SP1 molecules on mica and on silicon substrates, it is clear that the silicon substrate is more attractive to SP1 molecules since the number of SP1 molecules bound to silicon is higher than that bound to mica. Although the samples have been prepared under the same conditions as explained in chapter two. From the height profiles of some SP1 molecules on silicon, it was found that these molecules have a diameter ranges from 30 nm to 40 nm, while the heights range from 1 nm to 5.3 nm, Fig. 3.4.

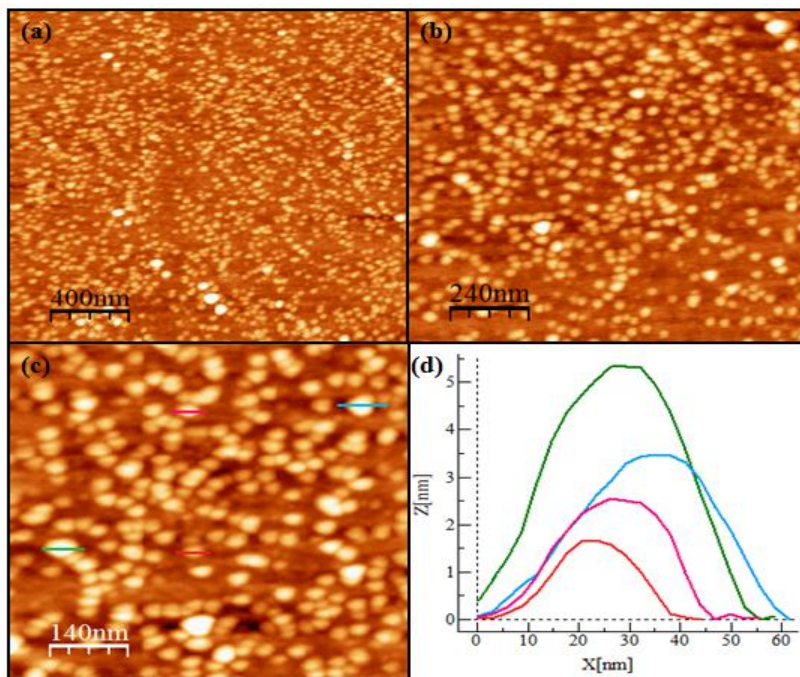


Fig. 3.4: AFM topography images of 73Cys-SP1 molecules on silicon substrate on different areas, acquired in tapping mode: (a) $2 \times 2 \mu\text{m}^2$, (b) $1.2 \times 1.2 \mu\text{m}^2$, (c) $700 \times 700 \text{ nm}^2$, and (d) height profiles of SP1 molecules.

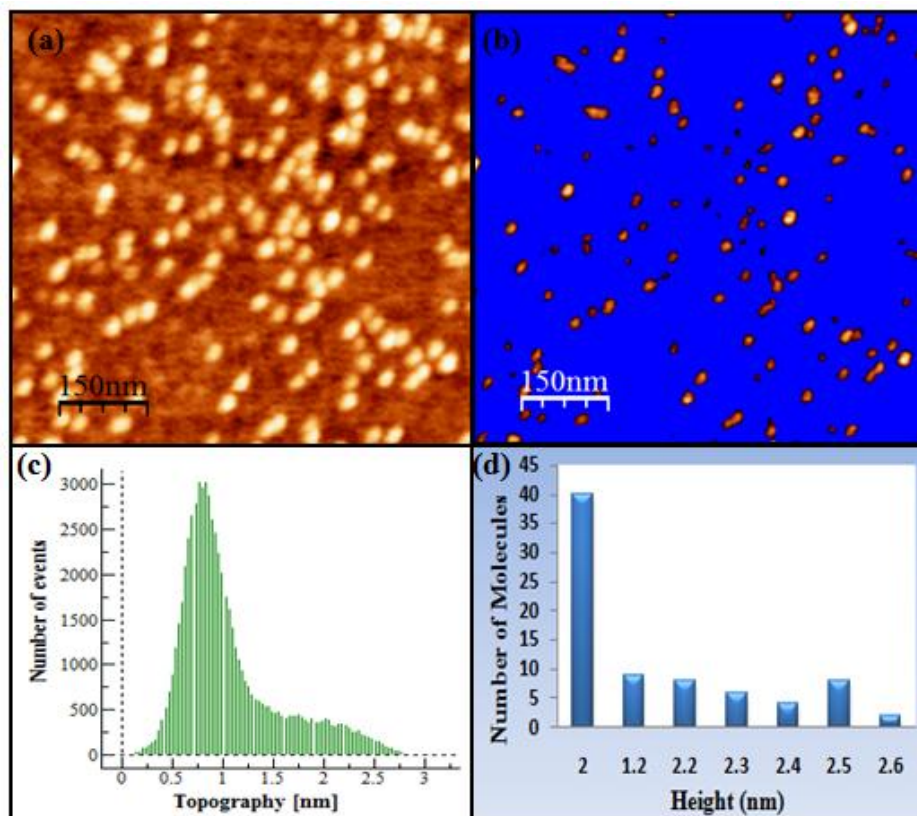


Fig. 3.5: (a) AFM topography image of 73Cys-SP1 molecules on silicon substrate, (b) flooding image of the topography (a) shows the SP1 molecules with heights range from 2 nm to 2.6 nm, (c) height distribution for the SP1 molecules in image (a), and (d) histogram shows height distribution of SP1 molecules in the flooding image (b).

The height distribution and the flooding image in Fig. 3.5, (b) and (c), performed on the topography image in Fig. 3.5a, shows that most of the heights are limited in the range (0.6 – 1.4) nm, and small number of objects with heights (2 – 2.6) nm are presented in the distribution tail, which indicates the presence of SP1 molecules in addition to SP1 fractions. The heights histogram of the flooding image shows that most of SP1 molecules (40 molecule) are of height equal to 2 nm, while the average height was found to be 2.2 ± 0.2 nm.

3.2.3 Morphological characterization of 73Cys-SP1 molecules on gold substrate

The SP1 molecules on the annealed gold substrate were morphologically characterized using both dynamic and contact AFM modes. The same type of tip was used in the morphology characterizations. It is clear from the topography image Fig. 3.6a that the gold grains are completely covered with SP1 molecules. In order to find the height of SP1 layers on the annealed gold substrate, the AFM contact mode was used to scratch small areas (200x200 nm) on different places of the sample. Figure. 3.6, (b) and (e) show the height profiles which were performed between the scratched and unscratched areas. These height profiles show the formation of SP1 layers with average heights 2 ± 0.1 nm and 5 ± 0.2 nm above the gold surface, Fig. 3.6, (c) and (f). The height of 2 nm indicates the presence of SP1 monolayer, while the 5 nm represents the height of two layers of SP1 molecules.

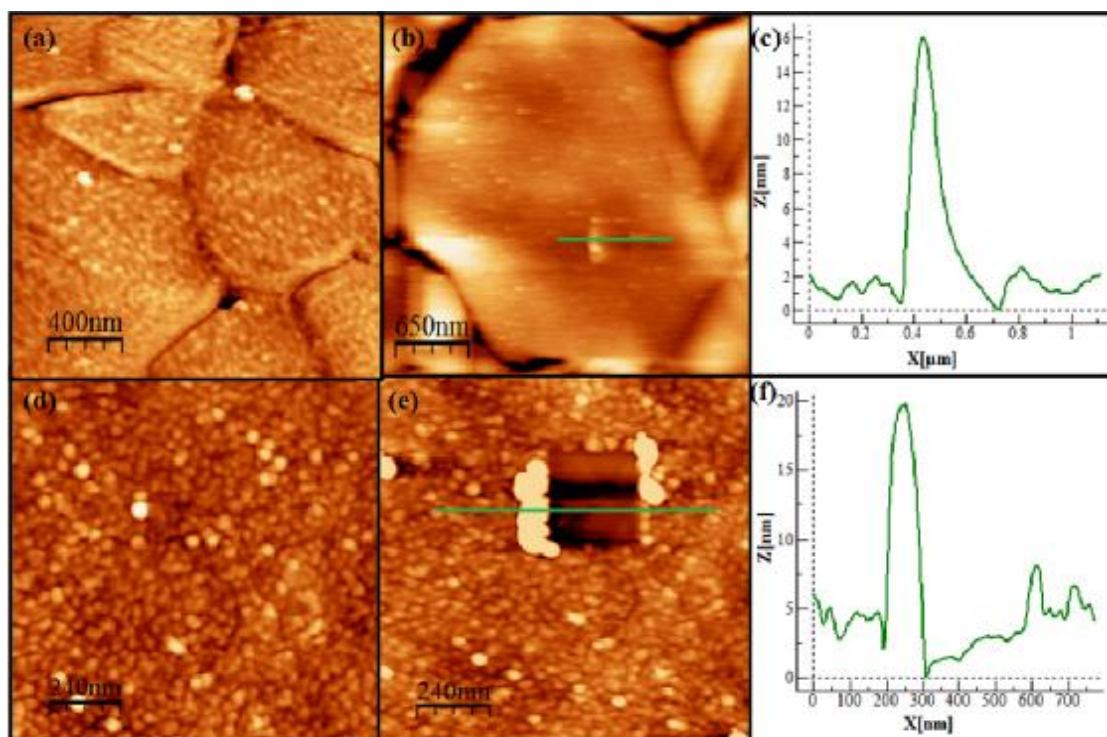


Fig. 3.6: AFM topography images of 73Cys-SP1 molecules on annealed gold substrate, on different areas, acquired in tapping and contact modes, the scratched regions were done using Si OMLC-AC tip, and the cross-section height profiles of the scratched areas: (a) $2 \times 2 \mu\text{m}^2$, (b) $3.2 \times 3.25 \mu\text{m}^2$, (d) and (e) $1.5 \times 1.5 \mu\text{m}^2$, (g) and (h) $1.2 \times 1.2 \mu\text{m}^2$.

3.2.4 Morphological characterization of 73Cys-SP1 molecules on HOPG substrate

The surface morphology of SP1 molecules on HOPG substrate was done using AFM dynamic mode, and the ElectriMulti75-G type tip. Figure. 3.7 shows topography images for different areas of the sample and the height profile performed between the HOPG surface and the SP1 molecules.

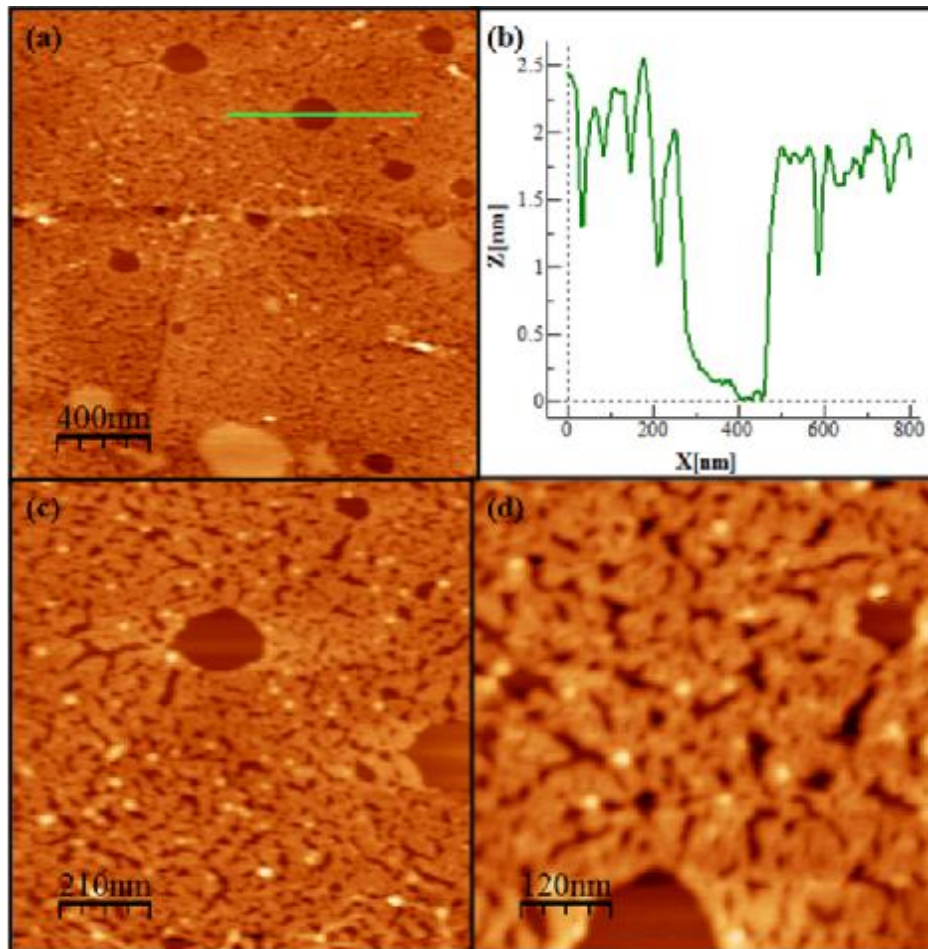


Fig. 3.7: *AFM topography images of 73Cys-SP1 molecules on HOPG substrate on different areas, acquired in tapping mode: (a) 2x2 μm^2 , (b) height profile of SP1 monolayer above HOPG substrate, (c) 1.1 μm^2 , and (d) 600x600 nm.*

The SP1 molecules spread on the HOPG surface to cover large areas, and leaving small parts in the shape of circles. The height profile which was performed between HOPG surface, i.e., the empty circle, and the SP1 molecules revealed that the average height of the SP1 molecules is 2 ± 0.1 nm, which is compatible with the height of the SP1 monolayer on the annealed gold substrate.

3.3.5 Morphological characterization of 6His-SP1-GNP molecules on mica substrate

AFM tapping mode with OMLC-AC tip were used to obtain the topographic images of SP1-GNP molecules on mica substrate. Figure. 3.8 shows SP1-GNP molecules on mica substrate, and the height profiles of some molecules, which revealed that these molecules have a diameter ranges from 21 nm to 23 nm, and heights range from 4.4 nm to 10.7 nm.

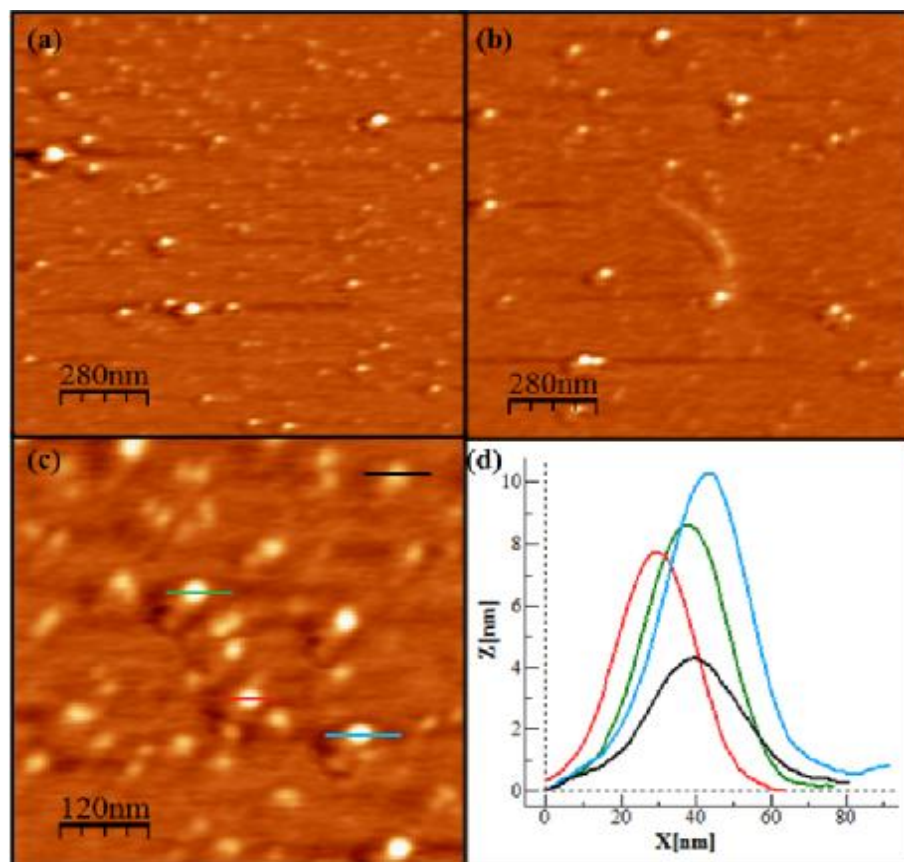


Fig. 3.8: AFM topography images of 6His-SP1-GNP molecules on mica substrate on different areas, acquired in tapping mode: (a) and (b) $1.4 \times 1.4 \mu\text{m}^2$, (c) $600 \times 600 \text{ nm}^2$, and (d) height profiles of 6His-SP1-GNP molecules.

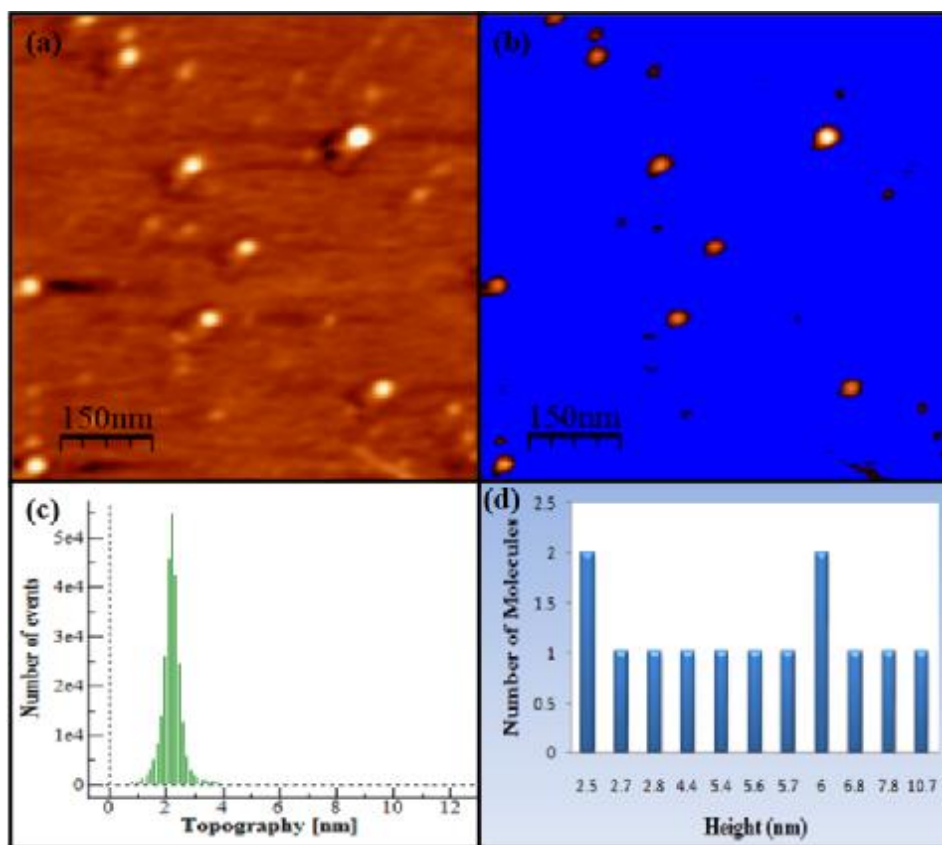


Fig. 3.9: (a) AFM topography image of 6His-SP1-GNP molecules on mica substrate, (b) flooding image of the topography (a) shows the SP1-GNP molecules with heights range from 2.5 nm to 10.7 nm, (c) height distribution for the SP1-GNP molecules in image (a), and (d) histogram shows height distribution of the SP1-GNP molecules in the flooding image (b).

The results obtained from the height distribution and the flooding image Fig. 3.9, (b) and (c), shows that most of the heights are limited in the range (2 - 2.5) nm. The heights histogram of the flooding image shows that the SP1-GNP molecules spread over the mica with different heights starting from 2 nm to 10.7 nm, while the height profiles which were performed on tens of molecules lead to average height equal 3.7 ± 0.4 nm.

3.2.6 Morphological characterization of 6His-SP1-GNP molecules on silicon substrate

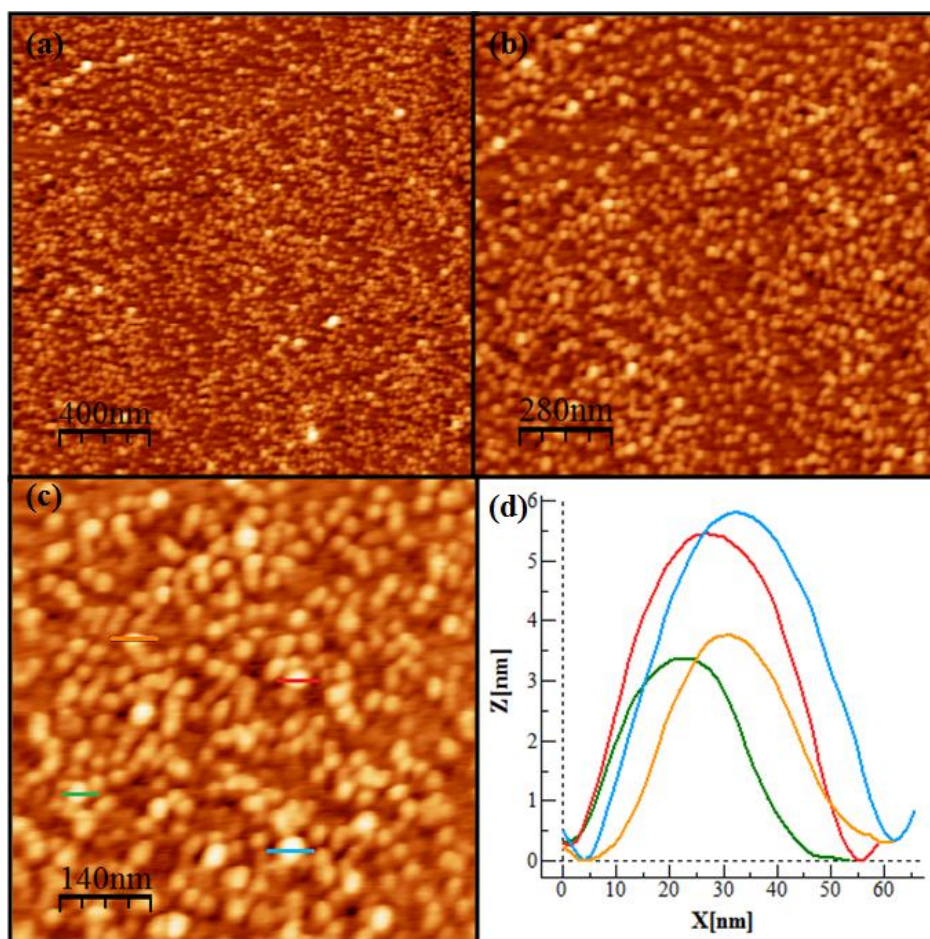


Fig. 3.10: AFM topography images of 6His-SP1-GNP molecules on silicon substrate on different areas, acquired in tapping mode: (a) $2 \times 2 \mu\text{m}^2$, (b) $1.4 \times 1.4 \mu\text{m}^2$, (c) $700 \times 700 \text{ nm}^2$, and (d) height profiles of 6His-SP1-GNP molecules.

The surface morphology on silicon substrate was characterized using AFM tapping mode with OMLC-AC tip. Although the samples on both mica and silicon substrates have been prepared under the same conditions but the difference between the number of SP1-GNP molecules that bound to both substrates is clear from the different topographic images performed on the two surfaces. From the height profiles, Fig. 3.10d, of some SP1 molecules on silicon, it was found that these molecules have a diameter ranges from 23 nm to 27 nm, while the heights range from 1 nm to 5.3 nm.

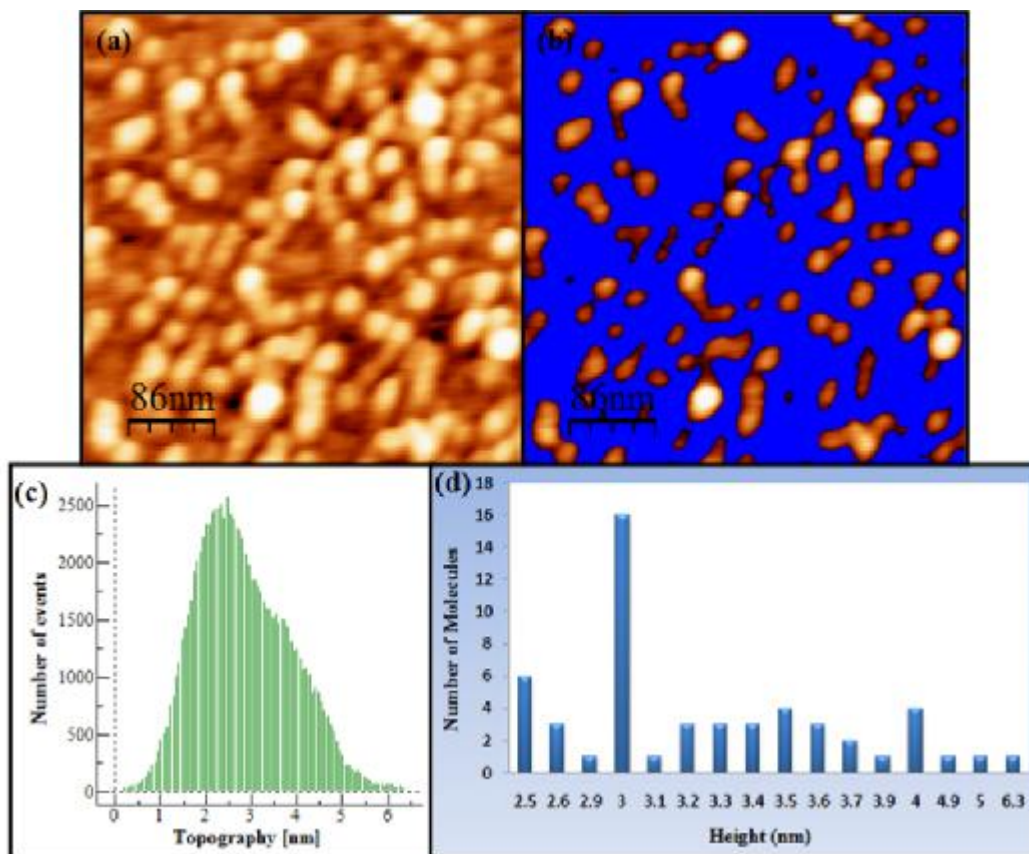


Fig. 3.11: (a) AFM topography image of 6His-SP1-GNP molecules on silicon substrate, (b) flooding image of the topography (a) shows the SP1 molecules with heights range from 2.5 nm to 6.3 nm, (c) height distribution for the SP1-GNP molecules in image (a), and (d) histogram shows height distribution of SP1-GNP molecules in the flooding image (b).

The height distribution of the topography image (a) in Fig. 3.11, shows the heights of the SP1-GNP molecules extended from 2 nm to 6 nm, which is identical with the heights histogram obtained for the molecules existed in the flooding image. The performance of several height profiles on many SP1-GNP molecules lead to average height equal to 3.3 ± 0.1 nm.

3.2.7 Morphological characterization of 6His-SP1-GNP molecules on gold substrate

The SP1-GNP molecules on the annealed gold substrate were morphologically characterized using both dynamic and contact AFM modes, and ElectriMulti75-G tip. Fig. 3.12 shows some topographic images for the annealed gold grains covered with SP1-GNP molecules. The height profile performed between the SP1-GNP's and the scratched area (200x200 nm) shows the average height of 4 ± 0.2 nm which indicates the formation of SP1-GNP monolayer on the gold substrate. The comparison between the heights obtained from the SP1 molecules for one monolayer on the annealed gold substrate (2 nm) and the height of the SP1-GNP monolayer (4 nm) is a proof of the existence of GNP's in the cavity of the SP1 molecules.

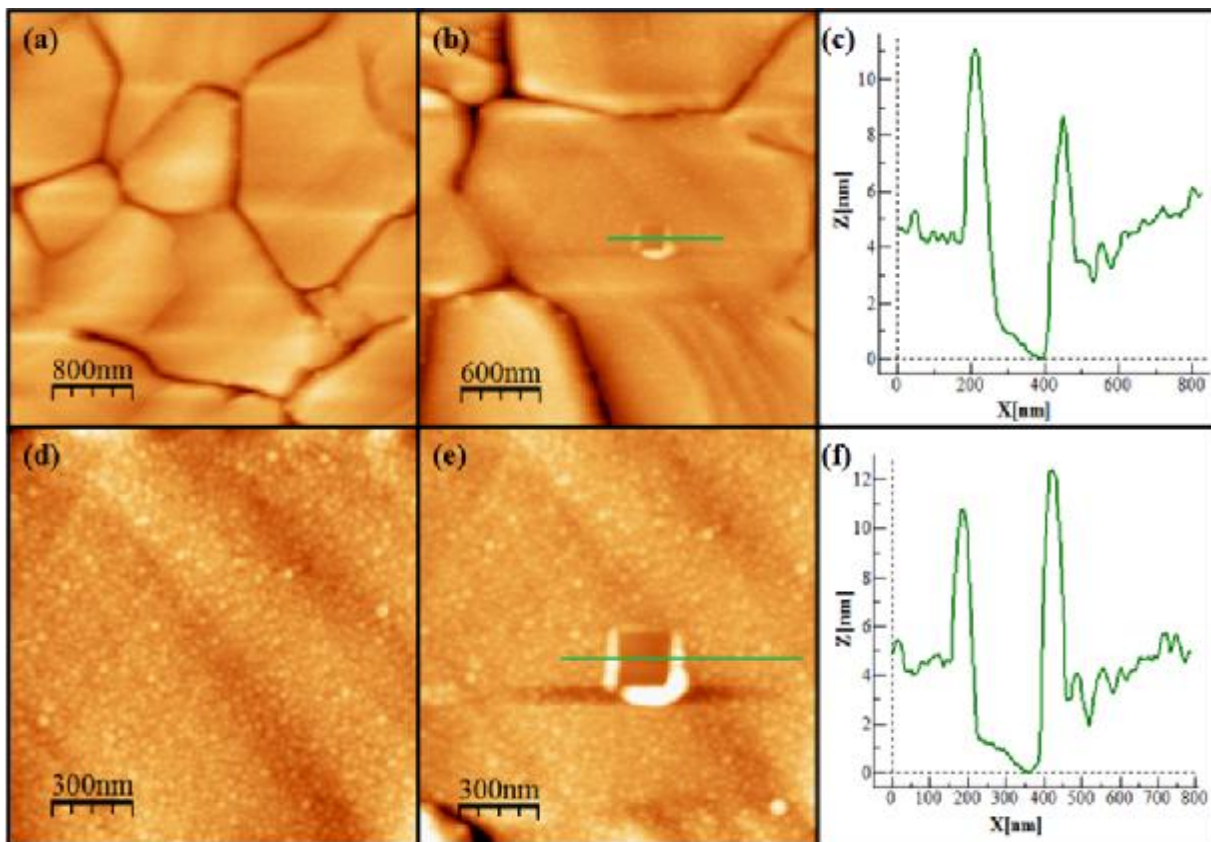


Fig. 3.12: AFM topography images of 6His-SP1-GNP molecules on annealed gold substrate, on different areas, acquired in tapping and contact modes, the scratched region was done using Si ElectriMulti75-G tip, and the cross-section height profile of the scratched area: (a) $4 \times 4 \mu\text{m}^2$, (b) $3 \times 3 \mu\text{m}^2$, (d) and (e) $1.5 \times 1.5 \mu\text{m}^2$.

3.2.8 Morphological characterization of 6His-SP1-GNP molecules on HOPG substrate

The surface morphology of SP1-GNP molecules on HOPG substrate was done using tapping and contact AFM modes. ElectriMulti75-G tip was used to perform the topography images and the scratching. Figure. 3.7 shows topography images for different areas of the sample and the height profile performed between the SP1-GNP molecules and the scratched area (200x200 nm).

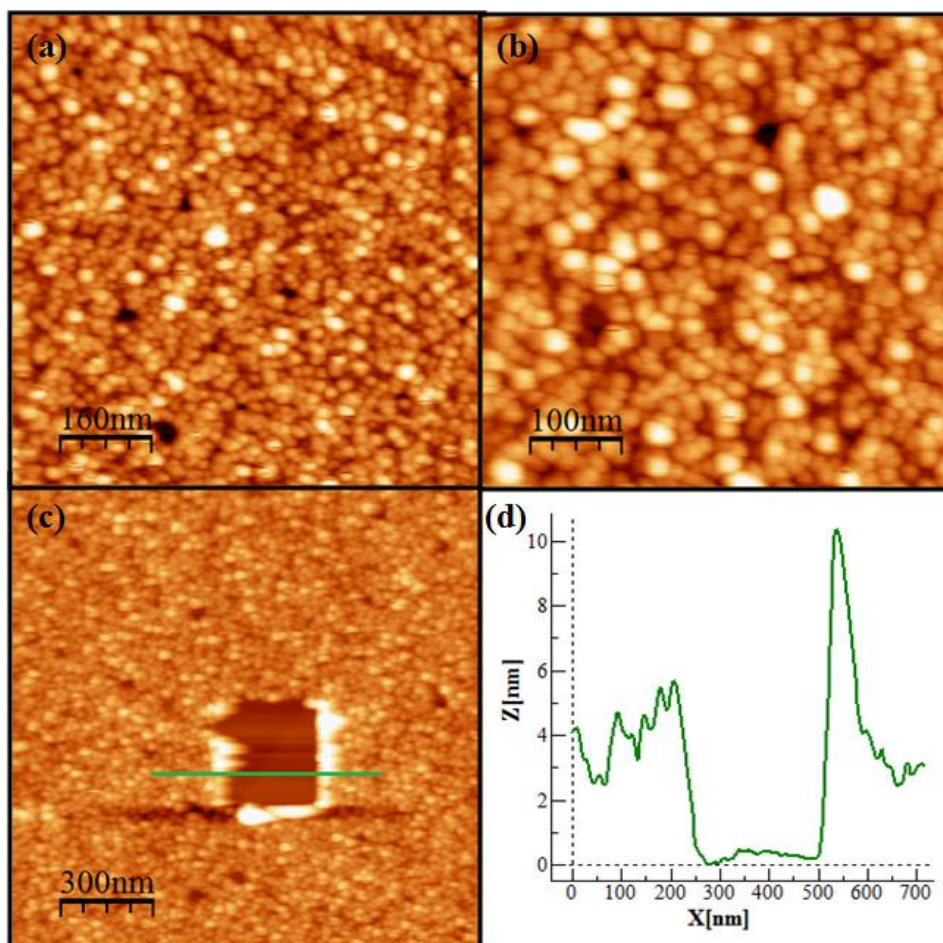


Fig. 3.13: AFM topography images of 6His-SP1-GNP molecules on HOPG substrate, on different areas, acquired in tapping and contact modes, the scratched region was done using Si ElectriMulti75-G tip, and the cross-section height profile of the scratched area: (a) $800 \times 800 \text{ nm}^2$, (b) $500 \times 500 \text{ nm}^2$, and (c) $1.5 \times 1.5 \mu\text{m}^2$.

The average height of the SP1-GNP layer was found to be 4 ± 0.2 nm above the HOPG surface, which is compatible with the height observed from the SP1-GNP molecules on the annealed gold substrate. The incubation time for this sample is (1 minute) which is less than that prepared on the annealed gold substrate (5 minutes) with the same concentration for both samples, which strengthen the assumption that the HOPG substrate is highly attractive to the SP1 molecules.

A comparison between the results obtained for SP1 and SP1-GNP dimensions by three different methods is illustrated in Table 3.1, While the comparison of the morphological results obtained for SP1 and SP1-GNP molecules on the different four substrates through this research is presented in Table 3.2.

Table 3.1: The dimensions of SP1 and SP1-GNP molecules obtained by different methods.

Method	SP1 diameter (nm)	SP1 height (nm)	SP1-GNP height (nm)
X-ray crystallography	11	4-5	-----
AFM tapping mode results on mica obtained by Medalsy with tip apex ~1nm	13 ± 1	2.3 ± 0.2	3.3 ± 0.2
AFM tapping mode results on mica obtained in this study with tip apex ~15nm	34 ± 0.3	2.4 ± 0.3	3.7 ± 0.4

The difference between the obtained dimensions and heights of the SP1 protein and the X- ray crystallography measurements (Dgany 2004) came as a result of surface-protein and tip-protein interactions. The difference between the dimensions and heights of SP1 and SP1-GNP obtained through this study and the dimensions obtained by Medalsy et al (Medalsy 2008) is due to: (a) tip-protein interaction, (b) the difference of mutants that attached to the SP1 molecules, and (c) to the conditions of preparing the samples.

Table 3.2: The dimensions of SP1 and SP1-GNP molecules obtained by AFM tapping mode on different four substrates.

Substrate	SP1 diameter (nm)	SP1 height (nm)	SP1-GNP diameter (nm)	SP1-GNP height (nm)
Mica	34 ± 0.3	2.4 ± 0.3	22 ± 0.2	3.7 ± 0.4
Silicon	35 ± 0.2	2.2 ± 0.2	24 ± 0.4	3.3 ± 0.1
Annealed gold	-----	Monolayer 2 ± 0.1	-----	Monolayer 2 ± 0.1
HOPG	-----	Monolayer 4 ± 0.2	-----	Monolayer 4 ± 0.2

The difference between the obtained heights and the coverage of the SP1 and SP1-GNP absorbed on the different substrates is due to:

1- Surface-protein interaction:

a- Adsorption on hydrophilic surface

The experiments showed that the adsorption of the hydrophobic SP1 protein on mica which is negatively charged hydrophilic surface, was less than that on the hydrophobic surfaces which are silicon, annealed gold, and HOPG. The interactions between SP1 protein and mica surface mainly include electrostatic interactions (Horbett 1997). On mica surface, the rearrangement or orientation of the adsorbed SP1 molecules take place whereby the mobile regions of positive charge are brought near the hydrophilic mica to enable the molecules to bind relatively tightly to the surface.

b- Adsorption on hydrophobic surface

The hydrophobic interaction is the major interaction on the hydrophobic surfaces; silicon, annealed gold, and HOPG. When SP1 protein arrived at the hydrophobic surface, structure rearrangement occur in which the hydrophobic groups of the SP1 are exposed to interact with surface. These hydrophobic groups of the SP1 protein have a strong hydrophobic force with hydrophobic surface, which explains the coverage of the SP1 and SP1-GNP molecules of the hydrophobic surfaces.

2- Tip-protein interaction

The radius of curvature of the two tips that were used for the morphological characterization of SP1 and SP1-GNP molecules is 23 nm, which is greater than the size of the SP1 molecules (11 nm). The difference in dimensions between the tip and the SP1 molecules influenced the morphological characteristics. As the tip scans over the SP1, the sides of the tip make contact before the apex, and the feedback mechanism begins responding the SP1 molecule, which lead to broadening of the SP1 molecule.

The large heights of some SP1 molecules which were found on mica and silicon substrates (5.5 nm, Fig. 3.4d) and SP1-GNP molecules (6-10 nm, Fig. 3.10d and Fig. 3.8d) could represent SP1 and SP1-GNP standing tubes, i.e., number of molecules bound above each other as presented schematically in Fig. 3.14.

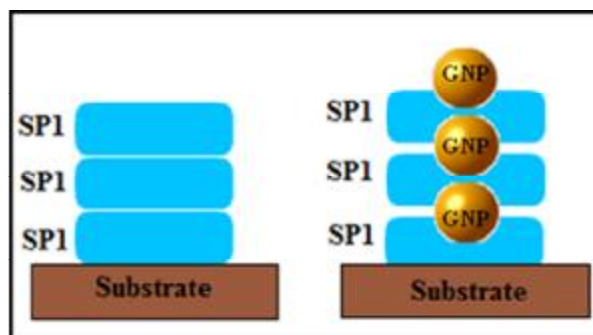


Fig. 3.14: A schematic of SP1 and SP1-GNP standing tubes.

3.3 Electrical characterization of 73Cys-SP1 and 6His-SP1-GNP molecules

The electrical characterization of SP1 and SP1-GNP molecules was measured by a C- AFM tip (ElectriMulti75-G), using Dulcinea electronics (Nanotec Electronica) as a voltage source and Keithley 6517A as an electrometer in the electrical circuit, as shown in the experimental setup, (see section 2.4).

Current-voltage measurements were combined with the force-distance mode which was described in chapter two. In F-d measurements, the distance between the oscillated tip and the sample was reduced in a pre-determined point above the sample while recording the tip deflection. The AFM software was modified to control the tip deflection (tip load on the sample) by limiting the approach at a fixed distance or when the amplitude reduction of the tip oscillations goes below a threshold. In the combined F-d/ I-V mode, the AFM software measures I-V curves in the last limited point of F-d (at the end of the approach cycle, before the withdrawal of the tip).

Current-voltage characteristics can be measured in different places along the F-d as in Fig. 3.15, meaning different height/ load (N.F) above the sample. In order to avoid tip-loading force on the sample, the approach can be stopped just before the “jump to contact” point of the F-d. The establishing of a good physical contact between the tip and the sample during the combined F-d/ I-V is proved by the presence of adhesion and capillary forces which can be observed on F-d curve, as seen in Fig. 3.15 (red lines).

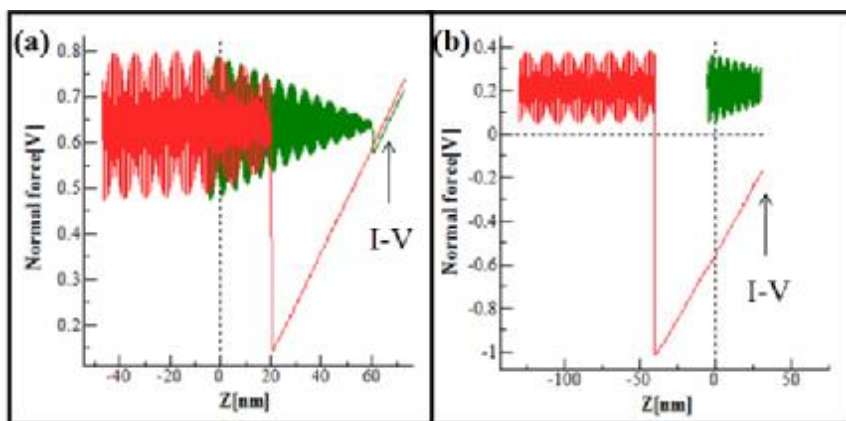


Fig. 3.15: *F-d* curves (a) with high load (N.F), (b) with small load (N.F) on bare gold; the green and red lines represent approach and withdrawal deflection of the oscillated tip respectively; in the last point of the approach, the I-V measurements can be performed; the slope of the red line in (b) shows the presence of adhesion and capillary forces between the tip and the gold

In the present work, *F-d* curves with small (Fig. 3.15b), and high load (N.F) (Fig. 3.15a) on the sample as in Fig. 3.15 were taken into account when comparing between the measurements. Current-voltage measurements on bare gold were done before and after the I-V measurements of the SP1 and SP1-GNP molecules as a validation of the tip conductivity. Fig. 3.16 shows the results of the combined *F-d*/ I-V mode on bare gold substrate.

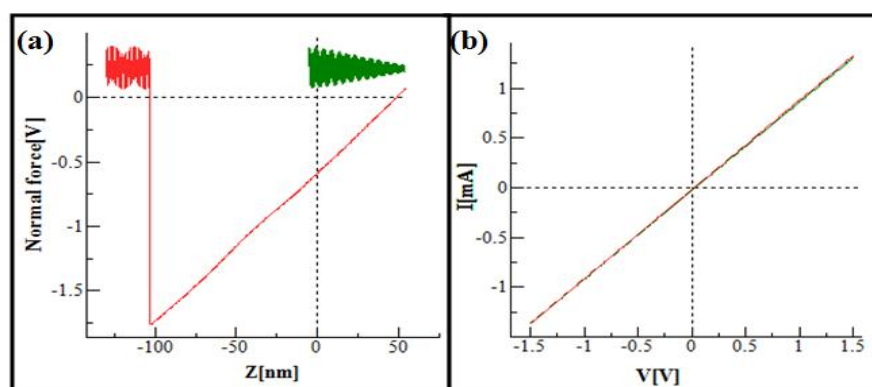


Fig. 3.16: Results of the combined *F-d*/I-V mode on bare gold, (a) *F-d* curve on gold with small load (N.F) of the tip on the sample, and (b) I-V curve for gold with voltage sweep from -1.5v to 1.5v.

Following the EFM results obtained by Medalsy, which revealed that the bare SP1 is electrically silent, while the SP1 gold hybrid is polarized (Medalsy 2008). Additional electrical measurements were done in order to understand the electron transport through these molecules, since the polarizability alone does not reflect the nature of these biological molecules and their electrical characteristics.

In the present work the I-V measurements of both SP1 and SP1-GNP molecules on HOPG substrate were checked several times and in several places with small and high load (N.F) on each sample.

Several I-V curves were collected for the SP1 molecules (height equal to 2 nm above the SP1 monolayer on the HOPG) with F-d curves, Fig. 3.17. Performing such F-d curves with small load (N.F) on the SP1 molecules will not affect their shape, and as a result, their electrical properties will not be changed.

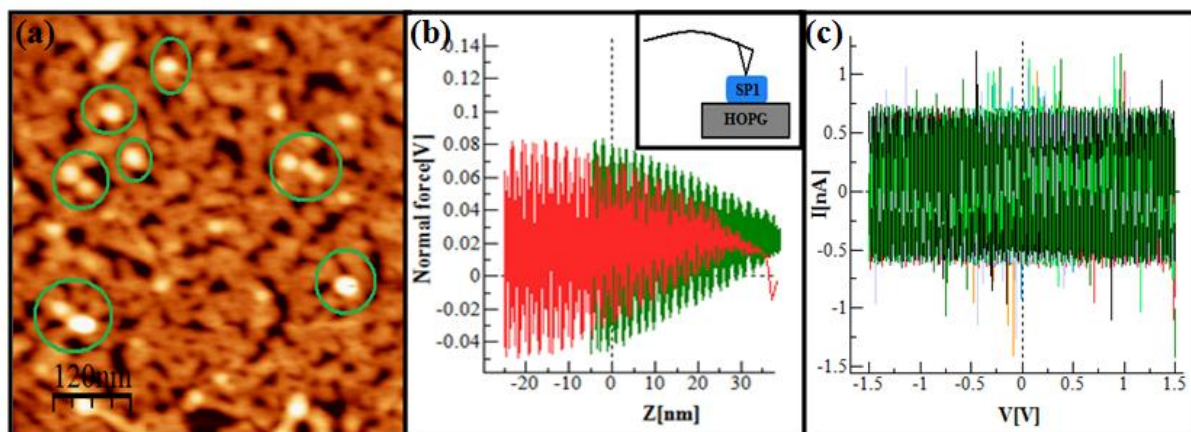


Fig. 3.17: Result of the combined F-d/I-V mode on SP1 molecules, (a) SP1 molecules that the measurements have been done on, (b) no pressing in F-d curve (green line), and (c) 10 I-V curves with zero current and voltage sweep from -1.5v to 1.5v.

In Fig. 3.17b the green line shows the absence of the “JIC” point, meaning small normal force on the SP1 molecules, while the red line in the withdrawal F-d curve indicates that a good contact was established between the tip and the SP1 molecules. Zero currents in Fig. 3.17c

demonstrate the insulating behavior of SP1 molecules. These graphs are representative of 10 measurements that were performed on SP1 molecules which are marked with green circles, Fig. 3.17a.

The measurements in a combined F-d/ I-V mode were done for SP1-GNP molecules in a similar way to the measurements on SP1 molecules. Fig. 3.18b shows an F-d curve, with no “JIC” point and with adhesion in the withdrawal. The I-V curves collected for SP1-GNP molecules which are marked in green circles are presented in Fig. 3.18c, which revealed an insulating behavior of SP1 gold hybrid.

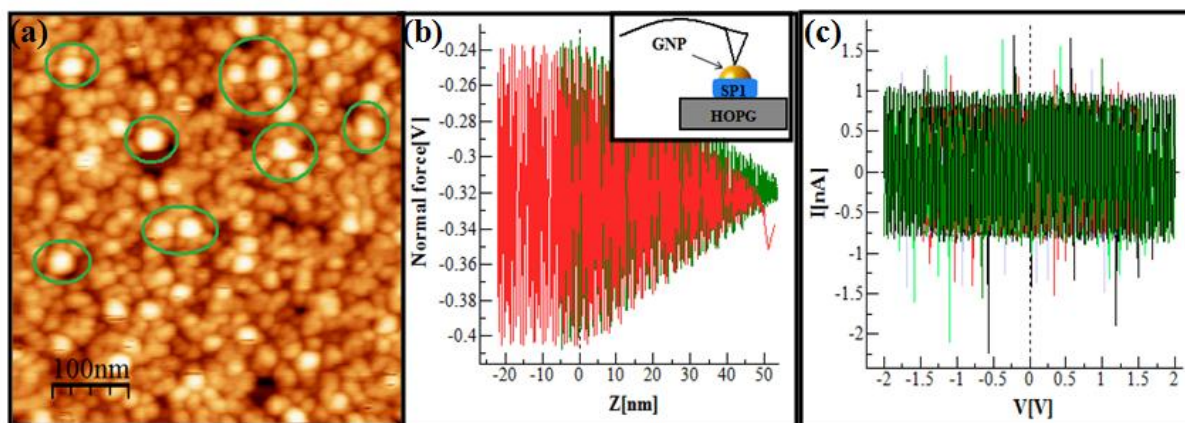


Fig. 3.18: Result of the combined F-d/I-V mode on SP1-GNP molecules showed, (a) SP1-GNP molecules that the measurements have been done on, (b) no pressing in F-d curve (green line), and (c) 10 I-V curves with zero current and voltage sweep from $-2v$ to $2v$.

Another I-V measurements were performed on both SP1 and SP1-GNP molecules using F-d curves with high load (N.F). Fig. 3.19 shows the F-d curve with the “JIC” point and some of the corresponding I-V measurements of the SP1 molecules.

Using F-d curves with high load (N.F) on the SP1 molecules caused them to be distorted and pressed toward the HOPG substrate making direct contact with it. The response of the SP1 molecules toward the applied bias lead to I-V curves having S shape or sigmoid shape which appeared in different bias ranges.

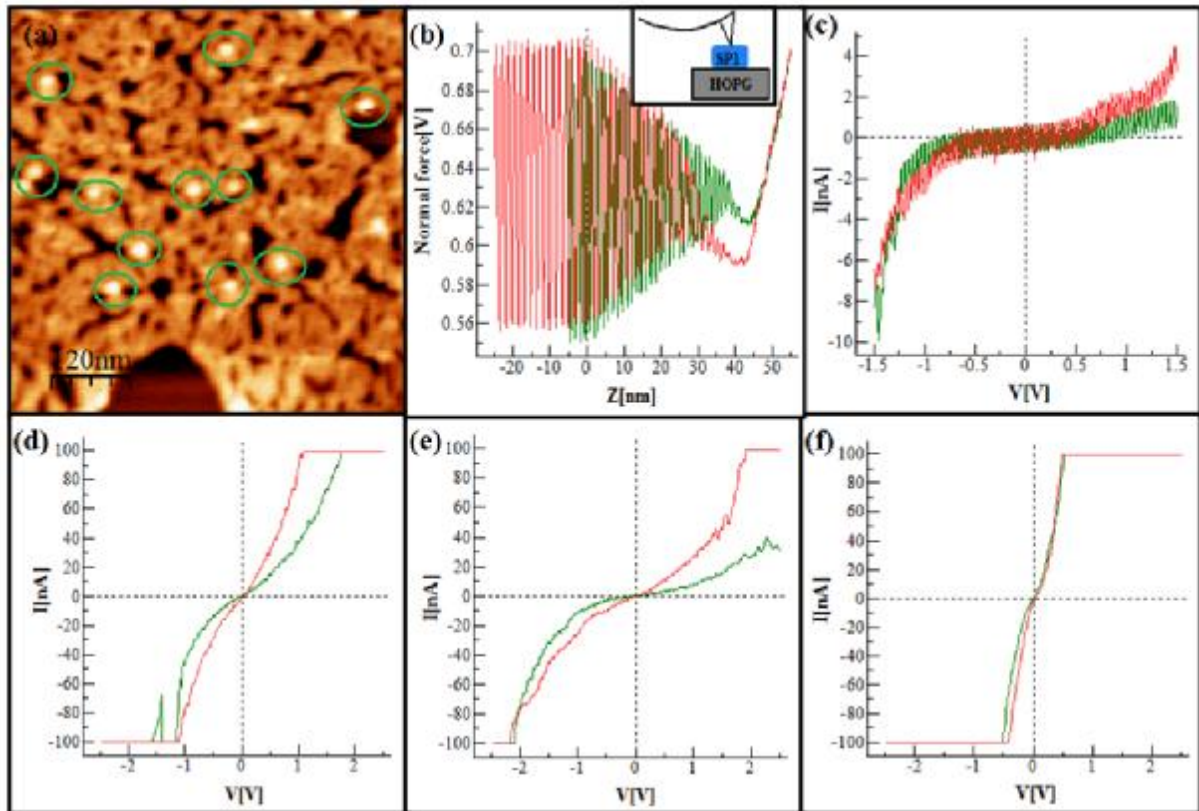


Fig. 3.19: Result of the combined F-d/I-V mode on SP1 molecules, (a) SP1 molecules that the measurements have been done on, (b) pressing in F-d curve, the SP1 molecule is pushed to direct contact with the HOPG substrate, and (c)-(f) the I-V curves with sweep voltage from -1.5v to 1.5v and -2v to 2v.

The same I-V measurements were performed for SP1-GNP molecules too with pressed F-d curves which result in pushing the GNP particles through the SP1 molecules and establishing direct contact with the HOPG substrate. Fig. 3.20 shows the pressed F-d curve and the corresponding ohmic I-V curves of the SP1-GNP molecules with voltage sweep from -2v to 2v.

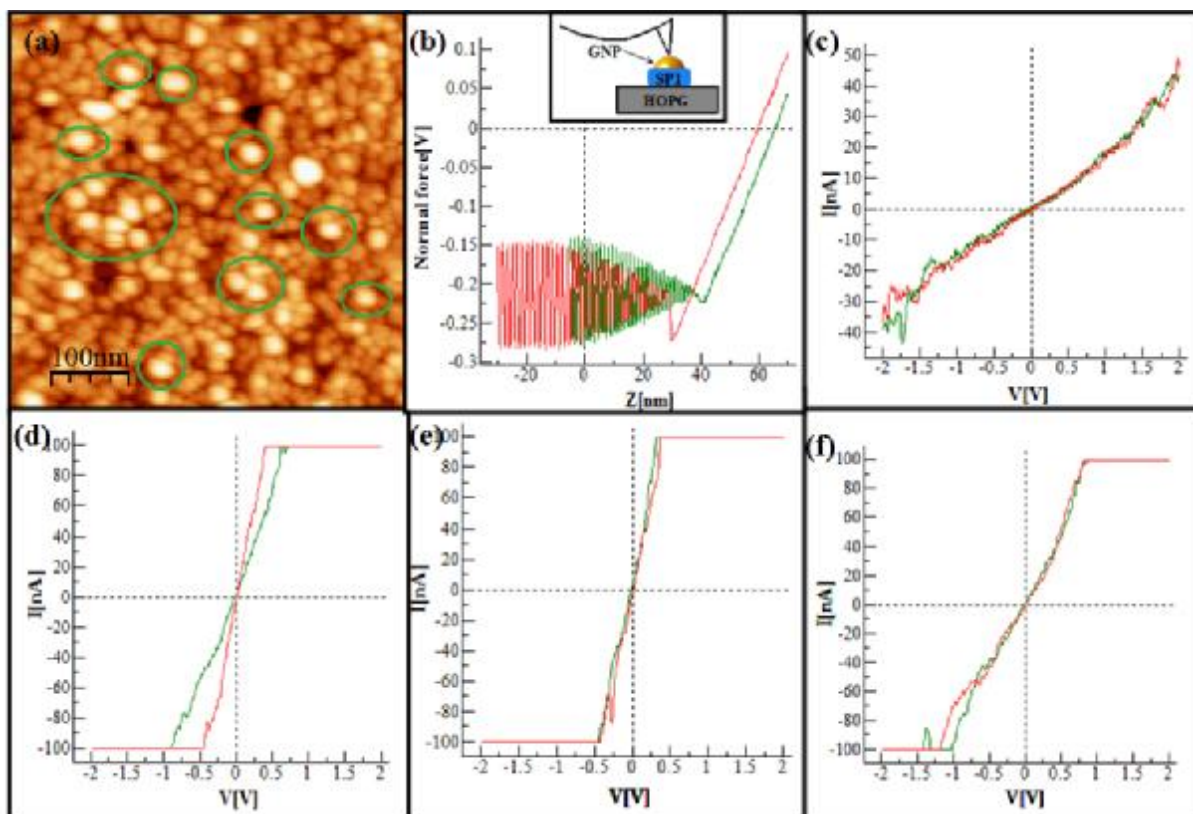


Fig. 3.20: Result of the combined F - d / I - V mode on SP1-GNP molecules, (a) SP1-GNP molecules that the measurements have been done on, (b) pressing in F - d curve, the GNP is pushed to direct contact with the HOPG substrate, and (c)-(f) the I - V curves with sweep voltage from $-2v$ to $2v$.

A comparison between the I - V s obtained from the SP1 and SP1-GNP molecules is presented in Fig. 3.21. The corresponding figures show the sigmoidal signal around the zero bias which is typical for organic contamination (ODA 2008), i.e., the SP1 molecule, and the ohmic signal which is identical for conductive substance, i.e., the GNP.

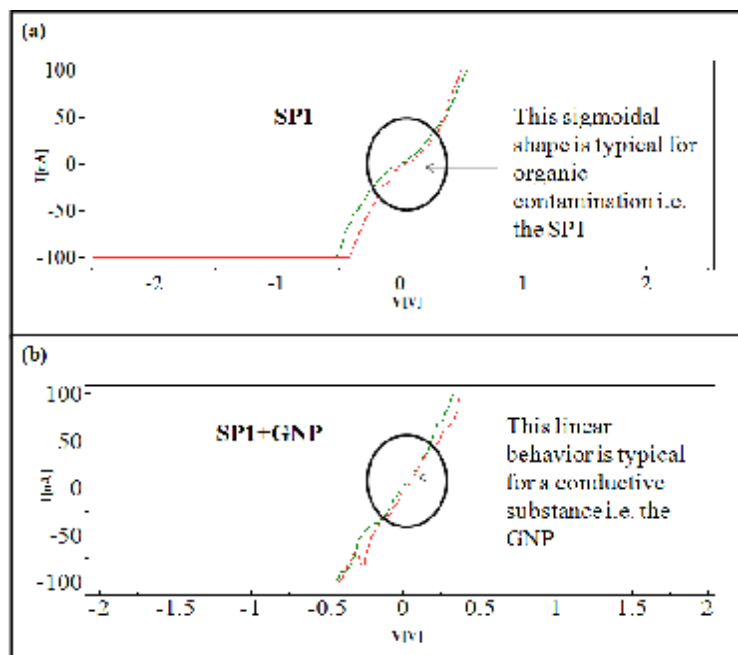


Fig. 3.21: A comparison between two I-V curves, (a) for SP1 molecule showing sigmoidal shape, (b) for SP1-GNP molecule showing an ohmic signal.

The great improvement of the SP1 and SP1-GNP molecules conductivity from I-V curve to another (in terms of conductance and current magnitude) may be a result of the great force applied on the SP1 and SP1-GNP molecules. The difference could also be due to a better contact between the tip and the molecules, or some other effect that has to do with the current, the temperature or the bias themselves. A comparison between the results obtained by the electrostatic force microscopy (Medalsy 2008), and the results obtained from the direct electrical measurements of this study is presented in Table 3.3.

Table 3.3: Electrical prosperities of SP1 and SP1-GNP molecules obtained by EFM and I-V.

Method	SP1 molecules	SP1-GNP molecules
Electrostatic force microscopy	Electrically silent	Polarized
Current-voltage with small load F-d curves	Insulator	Insulator
Current-voltage with big load F-d curves	Sigmoidal signal	Ohmic signal

The electrostatic force microscopy results which revealed that the SP1 molecules is not polarized have been done under specific condition which is the voltage value (from -5v to 5v). The direct electrical measurements shows a semiconductor behavior of the SP1 molecules, this behavior can be explained by the metal-protein-metal junction, as presented schematically in Fig. 3.22.

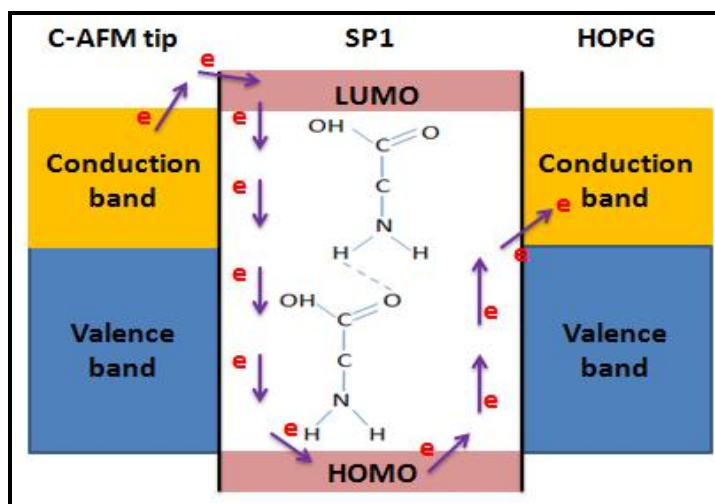


Fig. 3.22: A schematic of metal-protein-metal junction.

The SP1 protein has molecular orbitals, which are the Lowest Unoccupied molecular Orbital (LUMO) and the Highest Occupied Molecular Orbital (HOMO). When the C-AFM tip is connected to the SP1 protein, its conduction band has lower energy than the LUMO orbital of the SP1 molecule. By applying voltage, the electrons in the tip get an amount of energy that enables them to transfer to the SP1 LUMO orbital. After the injection of the charges through the SP1 molecule, these charges are distributed around the residue parts of the amino-acid. The charged amino-acid residues, the hydrogen bond between the amine and the acid, and the amide bond that is present along the polypeptide chain are considered as excellent candidates for hopping sites. So the charges transfer along the SP1 molecule through hopping until they reach the HOMO orbital. After that, the charges transfer to the conduction band of the HOPG substrate. This is one of the possible explanations that I thought about it to explain what could happen through the metal-protein-metal junction.

The electrical measurements of the SP1-GNP molecules show an ohmic behavior, which is identical to conductive substance; the gold nanoparticles. This ohmic behavior came as a result of the metal-metal-metal junction, since the tip pressed the GNP and lead to direct contact between it and the HOPG substrate.

The results obtained from the direct electrical measurements introduced the SP1-GNP as a basic building block for future nanoelectronic devices such as nanowires that can be performed by building SP1-GNP tubes as presented in Fig. 3.23. In this building block, the SP1 protein is used as incubator for the GNP, while the function of the GNP is electron transfer.

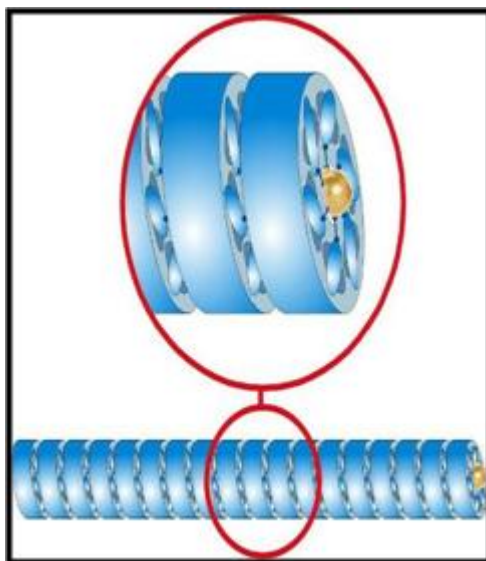


Fig 3.23: A schematic of a nanowire from SP1-GNP molecules.

Chapter FOUR

Conclusion and Future Work

Chapter Four

Conclusion and Future Work

4.1 Conclusion

In this research, morphological and electrical studies for the stable protein 1 (outer diameter 10 nm, inner diameter 4 nm and height 2.5 nm) and SP1 gold hybrid (gold nanoparticles are of dimensions equal to 1.8 nm) were done using AFM tapping, contact, and the combined F-d/I-V modes. Tapping mode AFM results for SP1 on mica, and silicon, showed an average heights equal to 2.4 ± 0.3 nm and 2.2 ± 0.2 nm respectively, while on gold, and HOPG substrates a monolayer of SP1 molecules was formed with average height equal to 2 ± 0.1 nm. The morphology of SP1-GNP molecules on the same substrates showed an average heights of 3.7 ± 0.4 nm and 3.3 ± 0.1 nm on mica and silicon, but on gold and HOPG a monolayer of average height equal to 4 ± 0.2 nm was formed.

The direct electrical measurements of SP1 molecules on HOPG substrate showed an insulating behavior with small load (N.F) F-d curves, and the same results were obtained for SP1-GNP molecules. The I-V measurements which were performed with high load (N.F) F-d curves showed a sigmoidal signal for SP1 molecules and an ohmic behavior for SP1-GNP molecules.

4.2 Future Work

The promising results in this work enhance the following future work:

- Building nanowires in a Lego like fabrication of nanoelectronic devices from SP1-GNP molecules.
- Measure a real conductivity in the constructed nanowires using electrical transport measurements.

References

References

[Bashir 2001] Bashir R. (2001): “**DNA-Mediated Artificial Nanobiostructures: State of The Art and Future Directions**”, Superlattices and Microstructures. Vol. **29**, No. 1, p. 1.

[Binnig 1986] Binnig G, Quate CF, and Gerber C. (1986): “**Atomic Force Microscope**”, **Phys. Rev. Lett. Vol. 56, p. 930.**

[Braun and Macdonald, 1982] Braun E, and Macdonald S. (Authors). (1982): “**Revolution in Miniature: The History and Impact of Semiconductor Electronics**”, second edition. The Press of the University of Cambridge, Cambridge.

[Dgany 2004] Dgany O, Gonzalez A, Sofer O, Wang W, Zolotnitsky G, Wolf A, Shoham Y, Altman A, Wolf S, Shoseyov O, and Almog O. (2004): “**The Structural Basis of the Thermostability of SP1, a Novel Plant (Populus tremula) Boiling Stable Protein**”, Journal of Biological Chemistry. Vol. **279**, No. 49, p. 51516.

[Drexler 1986] Drexler E. (Author). (1986): “**Engines of Creation: The Coming Era of Nanotechnology**”. Anchor Books, New York.

[Dummer 1997] Dummer G. (Author). (1997): “**Electronic Inventions and Discoveries**”, Fourth edition. Taylor & Francis, Inc.

[Dure 1993] Dure L, III. (1993): “**A repeating 11-Mer Amino Acid Motif and Plant Desiccation**”, Plant J. Vol. **3**, p. 363.

[Fabio 2004] Fabio P. (2004): “**A quantum mechanical study phosphotyrosyl peptide binding to the SH2 domain of p56^{lck} tyrosine kinase with insights into the biochemistry of intracellular signal transduction events**”, Biophys. Chem. Vol. **109**, p. 295.

[Feynman 1960] Feynman R. (1960): “**There’s Plenty of Rooms at the Bottom: an invitation to enter a new field of physics**”, *Eng.Sci.* Vol. **23**, p. 22.

[Geppert 1999] Geppert L. (1999): “**The 100-Million Transistor IC**”, IEEE Spectrum. Vol. **36**, p. 22.

[Hoerni 1961] Hoerni, J.A. (1961): “**Planar Silicon Diodes and Transistors**”, IEEE Transactions on Electron Devices. Vol. **8**, No. 2, p. 178.

[Horbett 1997] Horbett T, and Brash J. (1997): “**Protein at Interfaces II. Fundamentals and Applications**”, Journal of Controlled Release. Vol. 45, p. 113.

[Ingram 1996] Ingram J, and Bartels D. (1996): “**The Molecular Basis of Dehydration Tolerance in Plants**”, Annu. Rev. Plant Physiol. Plant Mol. Biol. Vol. **47**, p. 377.

[Iwai and Ohmi 2002] Iwai H, and Ohmi S. (2002): “**Silicon integrated circuit technology from past to future**”, Microelectronics Reliability. Vol. **42**, No. 4-5, p. 465.

[Maeda 1999] Maeda Y, Nakamura T, Uchimura K, Matsumoto T, Tabata H, and Kawai T. (1999): “**Controlled Conjugation of Nanoparticles with Single Stranded DNA**”, Vac. Sci. Technol. Vol. **17**, p. 494.

[McChesney 1994] McChesney R. (1994). “**Untitled review**”, The Journal of American History, Vol. **81**, No. 1, p. 310.

[McMillan 2002] McMillan R, Paavola C, Howard J, Chan S, Zaluzec N, and Trent J. (2002): “**Ordered Nanoparticle Arrays Formed on Engineered Chaperonin Protein Templates**”, Nature Materials. Vol. **1**, p. 247.

[Medalsy 2008] Medalsy I, Dgany O, Sowwan M, Cohen H, Yukashevskaya A, Wolf S, Wolf A, Koster A, Almog O, Marton I, Pouny Y, Altman A, Shoseyov O, and Porath D. (2008): “**SP1 Protein-Based Nanostructures and Arrays**”, Nano Lett. Vol. **8**, No. 2, p. 473.

[Moore 1965] Moore G. (1965): “**Cramming More Components Onto Integrated Circuits**”, Electronics. Vol. **38**, No. 8, p. 114.

[NOVA Workforce Board 2003] NOVA Workforce Board. (2003): “**Nanotechnology: The Next Great Wave of Innovation, White Paper**”.

(<http://www.novapic.org/lmi/reports/nanotech2003.pdf>, 17.07.2009)

[Oda 2008] Oda M, and Nakayama T. (2008): “**Energy-Level Alignment, Ionization, and Stability of Bio-amino Acids at Amino Acid/Si Junction**”, Jpn. J. Appl. Phy. Vol. **47**, No. 5, p. 3721.

[Pelah 1995] Pelah D, Shoseyov O, and Altman A. (1995): “**Characterization of BspA, A major Boiling-Stable, Water-Stress-Responsive Protein in Aspen (Populus Tremula)**”, Tree Physiol. Vol. **15**, No. 10, p. 673.

[Pelah 1997] Pelah D, Shoseyov O, Altman A, and Bartels D. (1997): “**Water-Stress Response in Aspen (Populus Tremula): Differential Accumulation of Dehydrin, Sucrose Synthase, GAPDH Homologues and Soluble Sugars**”, J. Plant Physiol. Vol. **151**, p. 96.

[Richter 2001] Richter J, Mertig M, Pompe W, Mönch I, and Schackert H. (2001): “**Construction of Highly Conductive Nanowires on a DNA Template**”, Appl. Phys. Lett. Vol. **78**, No. 4, p. 536.

[Rosenbloom and Spencer, 1996] Rosenbloom R, and Spencer W. (Editors). (1996): “**Engines of Innovation**”. Harvard Business School Press.

[Seeman 2003] Seeman N. (2003): “**Biochemistry and Structural DNA Nanotechnology: An Evolving Symbiotic Relationship**”, Biochemistry. Vol. **42**, No. 24, p. 7259.

[Sharma 2006] Sharma J, Chhabra R, Liu Y, Ke Y, and Yan H. (2006): “**DNA-Templated Self-Assembly of Two-Dimensional and Periodical Gold Nanoparticle Arrays**”, *Angew. Chem. Int. Ed.* Vol. **45**, p. 730.

[Shinar, Kafafi, and Vardeny, 1999] Shinar j, Kafafi Z, and Vardeny Z. (Editors). (1999): “**Optical and Electronic Properties of Fullerenes and Fullerene-Based Materials**”, First edition. Taylor & Francis, Inc.

[Taniguchi 1974] Taniguchi N. (1974): “**On the basic concept of nanotechnology**”, *Proc. Int. Conf. Prod. Eng.*, Tokyo. **Part. 2** (Tokyo: JSPE), p. 18.

[Thomashow 1999] Thomashow M. (1999): “**Plant Cold Acclimation: Freezing Tolerance Genes and Regulatory Mechanisms**”, *Annu. Rev. Plant Physiol. Plant Mol. Biol.* Vol. **50**, p. 571.

[Wang 2002] Wang X, Pelah D, Alergand T, Shoseyov O, and Altman A. (2002): “**Characterization Of Sp1, A Stress-Responsive, Boiling-Soluble, Homo-Oligomeric Protein From Aspen**”, *Plant Physiol.* Vol. **130**, p. 865.

[Wang 2003] Wang X, Dgany O, Dym O, Altman A, Shoseyov, O, and Almog O. (2003): “**Crystallization and Preliminary X-ray Crystallographic Analysis of SP1, A novel Chaperone-Like Protein Acta Crystallogr**”, *D Biol Crystallogr.* Vol. **59**, p. 512.

http://en.wikipedia.org/wiki/File:Transistor_Count_and_Moore%27s_Law_-_2008.svg, 13.07.2009.

<http://probe.olympus-global.com/en/en/specptE.html>, 12.06.2009.

http://www.sigmaaldrich.com/catalog/ProductDetail.do?N4=Z566675|ALDRICH&N5=SEARCH_CONCAT_PNO|BRAND_KEY&F=SPEC, 12.06.2009.

<http://www.e13.physik.tu-muenchen.de/Muellerb/AFMandSFM.htm>, 13.07.2009

المخلص

خلال العقد الأخير اكتسبت الجزيئات الحيوية اهتماما كبيرا في مجال تصنيع القطع الالكترونية, و ذلك بسبب الحاجة إلى قطع الكترونية جديدة بخصائص معينة, تتغلب و تتفوق على مساوئ الطرق الأخرى المستخدمة في تصنيعها. إن بناء قطع الكترونية باستخدام جزيئات حيوية يتطلب دراسة و فهم كيفية انتقال الإلكترونات خلالها. يقوم هذا البحث على دراسة الخصائص المورفولوجية و الخصائص الكهربائية لنوع من البروتينات ذو شكل حلقي يسمى البروتين المستقر 1, و لوحدة أساسية مكونة من جزيئات ذهب مزروعة في مركز هذا البروتين. تمت الدراسة المورفولوجية على أربعة أسطح مختلفة هي: الماكا, السيليكون, الذهب, و الجرافايت, و ذلك باستخدام مجهر القوى الذرية. أما دراسة الخصائص الكهربائية فقد تمت عن طريق عمل قياسات مباشرة من التيار و الجهد على البروتين والوحدات الأساسية و هي مرتبطة على سطح الجرافايت, و ذلك باستخدام تقنية قياسات مجهر القوى الذرية الموصلة.

أظهرت نتائج مجهر القوى الذرية بأن معدل ارتفاع البروتين على سطحي الماكا و السيليكون هو 2.4 ± 0.3 نانومتر و 2.2 ± 0.2 نانومتر على التوالي, بينما تكونت طبقة واحدة من هذا البروتين على سطحي الذهب و الجرافايت, وكان ارتفاع هذه الطبقة 2 ± 0.1 نانومتر. أما بالنسبة للوحدات الأساسية المكونة من البروتين و جزيئ الذهب , فقد أظهرت الدراسة بأن معدل الارتفاعات هو 3.7 ± 0.4 نانومتر و 3.3 ± 0.1 نانومتر على سطحي الماكا و السيليكون, على التوالي. أما سطحي الذهب و الجرافايت فقد تكونت عليهما طبقة ارتفاعها 4 ± 0.2 نانومتر .

بينت النتائج الناشئة عن دراسة الخصائص الكهربائية بأن كلا من البروتين و الوحدات الأساسية لها سلوك المادة العازلة عندما كانت القوة المستخدمة على البروتين والوحدات الأساسية خلال إجراء القياسات قوة عادية ذات قيمة قليلة, أما عندما تم إعادة عمل القياسات مرة أخرى باستخدام قوة عادية ذات قيمة كبيرة على كلا من البروتين والوحدات الأساسية, أظهرت البروتينات سلوكا كهربائيا يشبه سلوك المواد شبه الموصلة, بينما الوحدات الأساسية كان لها سلوك الموصلات.